NITED STATES
ARTMENT OF
MMERCE
BLICATION

NBS TECHNICAL NOTE 565

ARPA-NBS Program of Research on High Temperature Materials and Laser Materials

Reporting Period
January 1 to June 30, 1970

U.S.
ARTMENT
OF
OMMERCE
National
Bureau
of
andards

UNITED STATES DEPARTMENT OF COMMERCE
Maurice H. Stans, Secretary
NATIONAL BUREAU OF STANDARDS • Lewis M. Branscomb, Director

NBS TECHNICAL NOTE 565

ISSUED JANUARY 1971

Nat. Bur. Stand. (U.S.), Tech. Note 565, 84 pages (Jan. 1971)
CODEN: NBTNA

ARPA-NBS Program of Research on High Temperature Materials and Laser Materials

Reporting Period
January 1 to June 30, 1970

Edited by A. D. Franklin and H. S. Bennett

Inorganic Materials Division
Institute for Materials Research
National Bureau of Standards
Washington, D.C. 20234

Supported by the
Advanced Research Projects Agency
of the Department of Defense

For sale by the Superintendent of Documents, U.S. Government Printing Office, Washington, D.C., 20402.
(Order by SD Catalog No. C 13.46:565). Price 75 cents.

TABLE OF CONTENTS

Table of Contents (continued)

ARPA-NBS PROGRAM OF
RESEARCH ON HIGH TEMPERATURE AND LASER MATERIALS
Work Performed at the National Bureau of Standards
Supported by the Advanced Research Projects Agency
Department of Defense
(ARPA Order 373-62)
Reporting Period 1 January to 30 June, 1970
High Temperature Materials Reports Edited by A. D. Franklin
Laser Materials Reports Edited by Herbert S. Bennett

Brief reviews are given of work performed during this reporting period on several problems in the areas of High Temperature Materials and Laser Materials. Under the High Temperature Materials extremely pure Al_2O_3 crystals have been prepared and analysed chemically with the aim of providing specimens for research on mass transport, electronic, and similar properties. Oxygen diffusion data on TiO_2, obtained by the gas uptake method, agree with literature values, and work is now proceeding on developing a sectioning technique for oxygen diffusion. The optical constants of titanium have been determined over the visible portion of the spectrum. Soft x-ray spectra, nmr data, Mössbauer spectra, magnetic susceptibility, and other probes of the electronic density of states have been determined for a group of diborides of the first-series transition metals (Sc, Ti, V, Cr, and Mn) and interpreted in terms of the d-electron contribution to the density of states near the Fermi level. Both this project and the previous one on the optical properties of titanium have been completed. Under Laser Materials, the measurement of bulk optical properties and chemical analyses of ruby and Nd-glass are complete. Several techniques for determining the Cr^{3+} content in laser ruby have been developed and shown to agree; with these, it has been shown that very little loss of Cr^{3+} occurs when ruby turns orange under optical (x-ray or γ-ray) irradiation. A theory of laser pulse-induced damage at foreign particles in Nd-glass has been worked out; it suggests that detection before damage might be easiest with pulses of microsecond or longer duration. A high-power Nd-glass laser, Q-switched, has been

purchased for damage studies. The beam characteristics, which must be properly controlled for meaningful damage threshold measurements, are currently being studied.

Key words: Aluminum oxide, band structure, borides, bulk optical properties, chemical analysis, chromium ions, corundum, crystal defects, crystal growth, density of states, diffusion, glass, high temperature materials, laser damage, laser degradation, laser glass, laser materials, mass transport, neodymium glass, optical properties, opto-elastic properties, oxides, ruby, rutile, titanium, titanium dioxide, transition metal.

1. INTRODUCTION

The National Bureau of Standards, with the support of the Advanced Research Projects Agency (Office of Materials Sciences) of the Department of Defense, is carrying out a program of research on High Temperature and Laser Materials. The overall objective of this program is to provide some of the key elements needed by DoD in its pursuit of new technology through research and development. These elements include:

i. The preparation and characterization of materials needed for critical studies where exacting criteria of chemical purity, crystalline perfection, etc. must be met if progress is to be made,

ii. The development of new measurement techniques where these are required, and the acquisition of critically-needed data on certain material properties, and:

iii. The elucidation of the basic mechanisms contributing to or limiting the use of materials under extreme conditions (e.g. high temperatures, high intensity laser light, etc.).

A summary of the results achieved in the period January 1 to June 30, 1970, is given here.

2. OBJECTIVES

The development of new technology is often limited by the properties of the available materials. New material development requires a great deal in the way of background information about the behavior of the materials of the given class, about data on their properties, about methods of preparation of research-worthy specimens, and about measurement techniques capable of operating in new realms of application.

In a program of this kind, economy demands that key areas where new knowledge is needed be identified, and the work focussed upon these. We have chosen to emphasize the key problems of matter transport, expecially

oxygen, in oxides, and the degradation of laser materials, especially but not exclusively neodymium-doped glass, under high-energy laser pulsing. The work on the Optical Constants of Titanium is completed, the study of the Properties of Refractory Borides will be continued on another program. APRA support for both is ended with this report.

The Report is divided into two parts, High Temperature Materials and Laser Materials. Each part will open with a brief summary of objectives and accomplishments, followed by detailed Project summaries.

3. HIGH TEMPERATURE MATERIALS PROGRAM

3.1. Objectives and Summary of Program in High Temperature Materials

3.1.1. Objectives

The operation of rocket and jet engines involves exposing metals at high temperatures to oxidizing conditions, and raises the problem of oxidation protection of high temperature refractory metal structural components. This same problem, currently for superalloy turbine blades, is posed again by jet engines. The oxidation protection of metals requires some form of barrier layer to prevent diffusion. This layer, either applied or developed by the early stages of oxidation itself, will most likely be an oxide, and will function to keep the metal and oxygen apart. It can work only if the diffusion rates of oxygen and metal atoms through the layer are small enough. Thus the strategy for the development of oxidation protection of otherwise susceptible metals at high temperatures will depend in part on being able to control the rates of diffusion, and therefore, in having data on the diffusion rates themselves.

Diffusion in oxides is important to other classes of DoD problems. Thus improvements in the reliability and efficiency of military communication, computer, and radar circuitry could be made if ceramic magnetic and ferroelectric components could be made more reproducible

and reliable. Because such important properties as initial susceptibility and coercive force of ferrites, and dielectric and peizoelectric properties of ceramic ferroelectrics, are very sensitive to the microstructural features (porosity, grain size) controlled by sintering, the strategy for improvement here requires control over sintering in these ceramics. The same is true of ballistic response of ceramic armor. The development of transparent armor requires new techniques for the suppression of grain growth during otherwise complete sintering, mainly of Al_2O_3.

Since sintering in ceramics is mainly brought about by diffusion processes, the development of successful, long-range strategies to meet these DoD needs rests in part on knowledge of the rates of diffusion of metal and oxygen atoms in oxides.

Reliable techniques for measuring oxygen diffusion rates are not yet available, and therefore reliable data for oxygen diffusion does not exist for any save a few oxides. Thus one objective of this program is to develop a reliable technique for measuring the rate of diffusion of oxygen in oxides.

Further, diffusion rates are notoriously sensitive to impurities, and strategies for control require knowledge of the basic rate in the pure material and of the way various classes of impurities influence it. This in turn requires very pure crystals for study. To date, almost no oxide crystals have been prepared pure enough to reveal the intrinsic diffusion rates. The second objective in this area is to prepare intrinsically pure crystals of those materials for which mass transport data is sorely needed. The first candidate has been Al_2O_3, an important constituent in many ceramics, in particular for ceramic armor.

3.1.2. Summary of Progress to Date

The work on the preparation of very pure Al_2O_3 crystals has now produced what appear to be the purest and, from a chemical viewpoint, best characterized oxide crystals yet made. These crystals are clearly

pushing the capabilities of the most sensitive techniques for chemical analysis. Specimens have been made available to Prof. Arthur Heuer of Case Western Reserve University, who plans to study oxygen diffusion in them with his newly-developed proton activation technique. Such a test may ultimately be the only way of determining whether these crystals have reached the goal in this work, sufficient purity to achieve intrinsic, as distinct from impurity-controlled, mass transport. In the meantime, modifications have been made to the apparatus and starting materials that should further lower the concentrations of the remaining major impurities, especially silicon. It is planned to offer a limited amount of these high purity crystals to other laboratories for use in critical studies.

In the work on the development of a technique for measurement of Diffusion Coefficients in Oxides, the mass spectrometer for analysis of the oxygen isotope ratio (our means for following the transport of the oxygen tracer) has now been completed and put to use. With it, determination has been made of the oxygen diffusion coefficient in TiO_2 at several temperatures and a fixed oxygen partial pressure, by analysing the exchange between gas and crystal. The agreement between these results and recent values in the literature is good and gives confidence that the portions of the system so far in operation are performing satisfactorily. Still to be completed is the technique for moving oxygen from ground-off sections of the crystal into the mass spectrometer, so that the oxygen tracer penetration profile may be determined.

The project under the Properties of Refractory Borides heading, which now leaves this Program, has produced data on soft x-ray spectra, low temperature electronic specific heat, boron nmr Knight shift, electric quadrupole coupling, and x-ray lattice parameters for the series of diborides ScB_2, TiB_2, VB_2, CrB_2, and (except for the soft x-ray spectra) MnB_2. Having such a complete set of data across the early part of the first transition series of metals has revealed distinct trends that can be correlated with atomic and physical properties. These, together with band structure calculations now in

progress, should help in developing a fundamental understanding of the properties of this class of compounds.

The determination of the Optical Constants of Titanium has been completed. Our results are in good agreement with the best work in progress elsewhere. From our results and those of other laboratories, it is possible to understand the influence which oxidation of the surface has had on measured values in the past. With the current results, the basis is available for work on such problems as the initial development of oxide films, in the early stages of oxidation of the metal and its alloys. The very sensitive ellipsometric techniques are used in these studies.

3.2. Project Summaries in High Temperature Materials

3.2.1. Diffusion in Oxides

3.2.1.1. Crystal Growth From Vapor

H. S. Parker and C. A. Harding
Inorganic Materials Division
Institute for Materials Research

The objectives of the program are, first, the growth of aluminum oxide mono- and bicrystals of sufficient physical perfection and chemical purity for use as research materials, second, the reduction of both cation and anion impurities to sufficiently low levels to permit meaningful property measurements at the intrinsic level and third, the extension of the technique to other materials of interest.

During this reporting period, considerable effort has been devoted to the further chemical characterization of our aluminum oxide vapor grown crystals. Because neutron activation analysis cannot detect some likely impurities in an Al_2O_3 matrix, spark source mass spectrometric analysis was used as an alternative technique. The results, together with the previously reported activation analysis results for comparison, are given in Table 1.

Table 1

Chemical Analyses of NBS Vapor Grown Al_2O_3

Element	level, parts per million weight	
	Activation Analysis	Mass Spectrometric
Cu	0.027 - 0.038	1
Ir	0.0005 - 0.002	n.d.
Mg	a/	1
Mn	~0.0005	0.2
Cr	n.d. (<1)	0.3
Sc	~0.015	<5
Si	b/	<10 c/
B	b/	<0.01
V	b/	0.1
Cl	n.d. (<0.1)	<10

Analyses performed by Spectrochemical and Activation Analysis Sections, NBS

a/ Interference, in Al_2O_3 matrix

b/ Cannot detect in Al_2O_3 matrix

c/ Possible interference

It should be emphasized that where a value is shown as "less than," it represents an upper limit and should not be interpreted as the actual level in the material. At the levels of purity indicated in Table 1, determination of the absolute amounts present is a formidable problem. For example, compare the copper and manganese values shown in the table as determined by the two techniques. Thus, although magnesium, chromium, silicon and vanadium may be present as impurities, the actual amounts present remain in doubt. It is possible, however, to compare samples on a relative basis as shown in Table 2, where the NBS alumina is compared with some of the best Czochralski grown ruby. Barium and strontium, not detected in the NBS vapor grown Al_2O_3 tend to vary over a considerable range in the Czochralski ruby. The section of this report entitled "Physical and Chemical Properties of Laser

Materials" by Cleek and Waxler, from which the values quoted here for ruby were taken, discusses this point further.

Table 2

Comparison of NBS Vapor Grown Al_2O_3 with Czochralski Grown Al_2O_3

Element	NBS Vapor Grown	Czochralski Grown
Activation Analysis		
	ppm by weight	
Cu	0.027	0.016
Ir	0.0005	0.041
Mn	~0.0005	0.0006
Sc	~0.015	n.d.
Ga	n.d.	<0.006
Ba	n.d.	1.74
Sr	n.d.	0.085
Mass Spectrometric Analysis		
	ppm by weight	
Cu	1	1
Mg	1	1
Mn	0.2	0.7
V	0.1	0.4
Si	<10[a/]	<20[a/]
B	<0.01	<0.01

a/ Possible interference

As can be seen, the NBS vapor grown Al_2O_3 is of higher overall purity. In spite of the discrepancies between the techniques and possible interference (see silicon, Table 2), on a relative basis the results should be valid.

In an attempt to place an upper limit on some classes of impurities, two other techniques have been utilized in cooperation with Dr. R. A. Forman of NBS. The first is a measurement of the bulk

magnetic susceptibility and its temperature dependence from 300 K to 2 K. This measurement should lump together all paramagnetic impurities in terms of a temperature dependent (Curie Law) paramagnetic contribution to the susceptibility. Previous measurements on commercial sapphire by this means have detected a paramagnetic contribution. No Curie Law dependent part of the susceptibility was found and the susceptibility of the sample remained virtually constant at a value of $0.318 \pm 0.002 \times 10^{-12}$ m^3/g from 300 K to 2 K. The limits of precision of the measurement allow us to set an upper bound of 3 ppm of $S = \frac{1}{2}$, $g = 2$ paramagnetic centers in the sample, which corresponds to the maximum errors in the measurement. In the same units commercial sapphire (not the Czochralski ruby discussed earlier) has been found to contain approximately 125 ppm of paramagnetic centers.

The second technique utilized is optical absorption from the vacuum ultraviolet to the near infrared. Polished specimens of 1 to 3 mm nominal thickness were used. The transmission was measured over the wavelength range of about 140 to 7000 nm. Over this range, no evidence of absorption bands were found. Calculations of the absorption coefficient, uncorrected for the higher reflection losses in the ultraviolet as compared to the visible spectrum, show that the absorption coefficient drops essentially to zero at a wavelength of 200 nm. This optical measurement should be extremely sensitive to most of the transition metals, which would display strong charge transfer bands in the ultraviolet region, and should be sensitive to many of the common anion impurities which might be expected such as OH^-. While these measurements do not allow us to give a limit on the concentration of impurities present, they indicate the extreme purity of the material.

Assembly of the new growth apparatus is currently in progress. It is hoped that the use of higher purity aluminum (99.9999%) together with the minimized contact of chlorine and aluminum chloride with exposed metal in the new apparatus will further reduce the impurity level in the vapor grown aluminum oxide.

A paper entitled "Vapor Growth of Bicrystals of Aluminum Oxide" has been accepted for publication in the Journal of the American Ceramic Society.

For the next reporting period, continued emphasis will be placed on reduction in impurity levels. Although it appears that it will be necessary to evaluate chemical purity on a relative basis at this stage, further investigation of possible methods of chemical characterization will be continued. The completion of the second, improved growth apparatus should make limited numbers of crystals of the high purity aluminum oxide available to a greater number of investigators.

3.2.1.2. Diffusion in Refractory Materials

A. L. Dragoo and F. P. Knudsen
Inorganic Materials Division
Institute for Materials Research

The objectives of this program are to measure and to interpret diffusion of oxygen in single crystal oxides. Experimentally these two objectives consist of (1) extending the sensitivity of present techniques so that the ^{18}O distribution in a single crystal sample can be measured, (2) comparing the results of these concentration profile measurements with measurements of the rate of exchange of ^{18}O between the gas phase and the oxide crystal, (3) determining the dependence of the diffusion rate on temperature, oxygen partial pressure, impurities in the solid, etc., and (4) obtaining reliable diffusion and exchange coefficients. In regard to interpretation, this objective translates into determining the mechanisms for oxide ion diffusion in the oxide studied. Currently, rutile (TiO_2) is the oxide of interest.

Since the previous report, the inlet system for the isotope ratio mass spectrometer has been completed. We have found it possible to analyze quantities of oxygen as small as 0.02 standard cc. Oxygen samples obtained from the diffusion furnace are on the order of 0.3 standard cc with a pressure in the furnace of about 3×10^4 N/m^2 (1/3 atm). The mass spectrometer and inlet system

were used in conjunction with the diffusion furnace to measure the diffusion coefficient reported below.

A diffusion anneal was carried out in a platinum tube diffusion chamber at 1275°C, at a pressure of 4.29×10^4 N/m^2 (0.424 atm) and for a duration of approximately 124 hours. Fifteen O_2 samples were taken from the diffusion chamber during this time and the decrease in ^{18}O-content of the gas (about 3% for the entire anneal) was analyzed to determine the diffusion coefficient.

For diffusion parallel to the c-axis of a single crystal rutile disc we obtained $D = 8.9 \times 10^{-12}$ cm^2/s.

This result agrees well with the result of Haul and Dümbgen[1] as did our previous result at 1350°C. Recent measurements [2] by Lees, Calvert, and Derry, using a resonance capture of protons to study oxygen diffusion in titanium dioxide, have yielded diffusion coefficients at 1000° and 1400°C which agree well with the results of Haul and Dümbgen. The sample used in the current study had about 20% of its surface covered with small platinum crystals by the time the anneal was terminated. The previous sample was annealed in an alumina tube and thus was not subjected to this interference. Haul and Dümbgen who carried out their measurements on rutile powders in platinum tubes experienced no platinum deposition.[3] We are currently investigating ways of eliminating this problem.

References

1. R. Haul and G. Dümbgen, J. Phys. Chem. Solids 26, 1 (1965).
2. D. G. Lees, J. M. Calvert, and D. J. Derry, "A technique using resonance capture of protons to study oxygen diffusion in titanium dioxide," paper presented at the Thomas Graham Memorial Symposium on Diffusion Processes, University of Strathclyde, Glasgow, Scotland, 1969.
3. R. Haul, private communication.

3.2.2. Properties of Refractory Borides

3.2.2.1. Electronic Structure of Refractory Hard Metals

J. R. Cuthill, L. H. Bennett, G. C. Carter
and A. J. McAlister
Metallurgy Division
Institute for Materials Research

The objective of this project is to study changes in the density of states upon compound formation, especially in high temperature borides. The information should contribute to the understanding of the basic principles leading to the design of high temperature alloys with prescribed properties. The class of compounds being considered in this study are those binary and pseudo-binary compounds characterized by one of the constituents having an incomplete d or f shell and the other constituent having no d or f electrons. The transition metal borides, aluminides, and beryllides are examples.

Information is being obtained in the present study from soft x-ray spectroscopy, nuclear magnetic resonance, Mössbauer spectroscopy, magnetic susceptibility, and other probes of the electronic density of states. The soft x-ray spectroscopy, nuclear magnetic resonance, and electronic structure calculation results obtained during this report period are as follows.

A series of boron-K valence band x-ray spectra obtained from the diborides in the first transition series, i.e. ScB_2, TiB_2, VB_2, and CrB_2 as well as from pure single crystal boron reveals some pronounced trends in the fine structure and shift in the maximum peak energy that appear to correlate with d-electron concentration and with melting point. The pure boron spectra peaks at about 185 eV. With increasing d-electron concentration the peak shifts downward in energy to 183 eV for the location of the boron-K peak in CrB_2 (see Figure 1). The trends in fine structure are also evident in Figure 1. The structure on the high energy edge (at "A") becomes increasingly more pronounced with increase in d-electron concentration, i.e. becoming most pronounced

in CrB_2. Meanwhile, the structure on the low energy side at "B" appears to show an intensity variation correlated with melting point of the diboride. There has been evidence of this peak shift and the fine structure on the high energy edge in boride spectra that have been reported on previously in the literature but this is the first time that data on the complete series has been obtained which, together with the results of the APW calculation of the band structures for these borides, should make the possibility of a fundamental interpretation of these data much more promising.

Work on the augmented plane wave calculations of the transition metal diboride band structures is continuing. A serious practical limitation to the extent of these estimates is posed by the large secular equations necessitated by the C32 cellular basis. In view of this, we have been forced to limit the scope of the work to state distribution calculations for CrB_2, using a reasonable crystal potential, with the aim of constructing a useful model of the electronic structure of the series via a semi-rigid band picture.

New data have been obtained for Knight shifts and electric quadrupole coupling constants. These, together with previous results, are plotted in Figure 2. This now shows some general trends of the NMR results, which fit in fairly well with data on electronic specific heats (also shown in Fig. 2), and susceptibilities, both of which show increased d-like contributions for the three compounds on the right hand side of the plot (CrB_2 becomes antiferromagnetic at $T_N \sim 86°K$, and MnB_2 becomes ferromagnetic at $T_c \sim 143°K$). Increased d-like contributions are also suggested by Hall effect and resistivity data. The increased d electron contribution is apparent in the Knight shift data as well: $K(Sc^{11}B_2) = 0.00(1)\%$ for the compound most to the left of the plot, with a steady decrease towards MnB_2 with $K = -0.05(3)\%$. This latter value was obtained using a sample which was analyzed to contain some 20% second phase. This second phase was apparent in the quadrupole spectrum in that more than one set of satellites were present, one of which gave a value of $\frac{e^2qQ}{h}$ close to that reported in

the literature. A value for the ^{11}B Knight shift in MnB_2 has not been previously reported. Our K value includes a contribution due to the second phase. However, the shape of the central line is rather broad ($\sim$ 35 gauss) and fairly symmetric. The central line shows no structure due to a second phase, but does have rather wide wings. We believe the actual K value to lie within the indicated range. The results on the ScB_2 samples are being prepared in final draft for publication.

The general results thus indicate increased d-electron contributions at (or near) the Fermi surface as one goes across the series ScB_2, TiB_2, VB_2, CrB_2, MnB_2. For the Knight shift results this means increased d-core polarization causing more negative Knight shifts. This is indeed observed (Fig.2b). The Knight shift at the metal site shows a similar trend: For ^{45}Sc in the diboride $K = +0.07\%$. This is a value reduced substantially from the metal value of 0.25%, but is still positive. For ^{51}V in VB_2, $K = -0.3\%$, and temperature independent. Usually, when d-core polarization is involved a temperature dependence is observed. No temperature dependence is reported for the $^{51}VB_2$ Knight shift however, and the susceptibility is also reported to be nearly temperature independent. The ^{11}B K values for these compounds are also all temperature independent, and a likely mechanism for producing the negative K values is that of inter-atomic exchange polarization. For the 2p incomplete valence shell p-core polarization is thought to be positive and therefore not the cause of negative $K(^{11}B)$ values.

The quadrupole coupling constants show a smooth trend (Fig. 2c) but their interpretation is still rather ambiguous. There seems to be no direct correlation with relative cell dimensions (Fig. 2d). There is a possibility that the boron atoms do not lie in flat hexagonal "rings", but are rather in a pleated, or puckered configuration, with every other boron atom above and below the plane of the "ring". If for these compounds such configurations are true, the quadrupole coupling constant would be affected, possibly causing this apparent lack of correlation between the e^2qQ/h, and c/a values. Such a puckered configuration is not easily observed as x-rays look at the transition

metal atoms, rather than the light boron atoms. Quadrupole effects in NMR also do not reveal an asymmetry parameter, as the three fold symmetry at the boron site is not destroyed by puckering.

NMR K and $\frac{e^2qQ}{h}$ values have also been measured in YB_2 for the first time. Again ^{11}B resonance has a near zero shift. The quadrupole coupling constant is 0.34(1) MHz and the central linewidth 8 gauss at 16 MHz and 7 gauss at 8 MHz (the line being somewhat asymmetric). These samples are maybe 75% of the YB_2 phase with several unidentified lines in the x-ray diffraction pattern. This explains the slight field dependence of the central linewidth. The Y nucleus has $I = \frac{1}{2}$ and therefore no satellites are observed. The central resonance in our samples was not simple, also indicating lack of single phase. The total width of the line was such that a Knight shift of + 0.3(2)% could be deduced, as measured using $^{39}KCOOH$ and $H^{14}NO_3$ as references, employing the values $\nu^{39}_{KCOOH}/\nu^{89}_{YCl_3} = 0.95247$ and $\nu^{14}_{HNO_3}/\nu^{89}_{YCl_3} = 1.47462$, respectively. These results are quite similar to those of ScB_2, which is isoelectronic to YB_2.

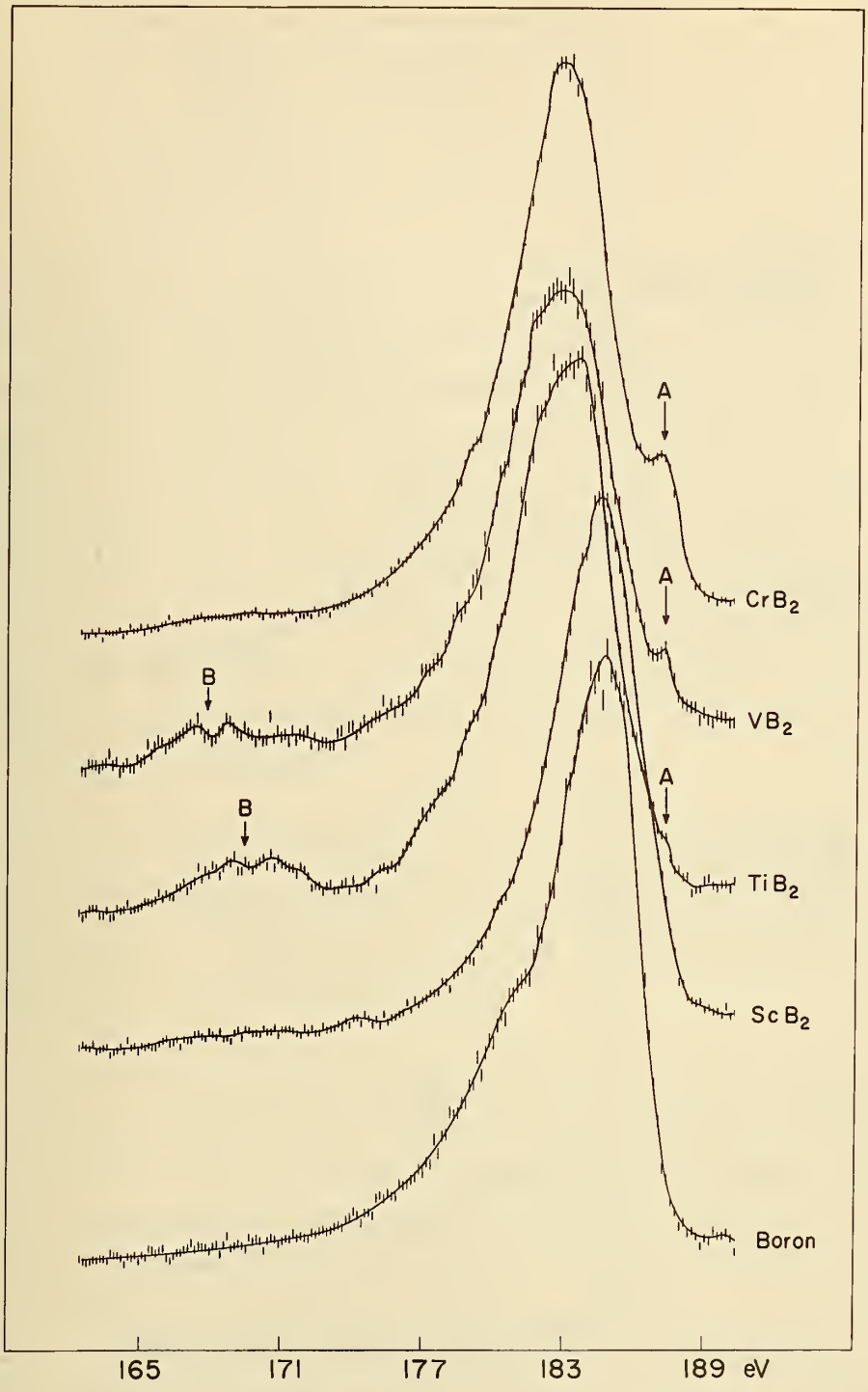

FIGURE 1. The boron-K emission spectrum from crystalline boron and from ScB_2, TiB_2, VB_2, and CrB_2. Based on the respective excitation current in each case, the specimen temperatures are estimated to be on the order 500°C ± 50 for the crystalline boron and 700°C ± 100 for the transition metal diborides.

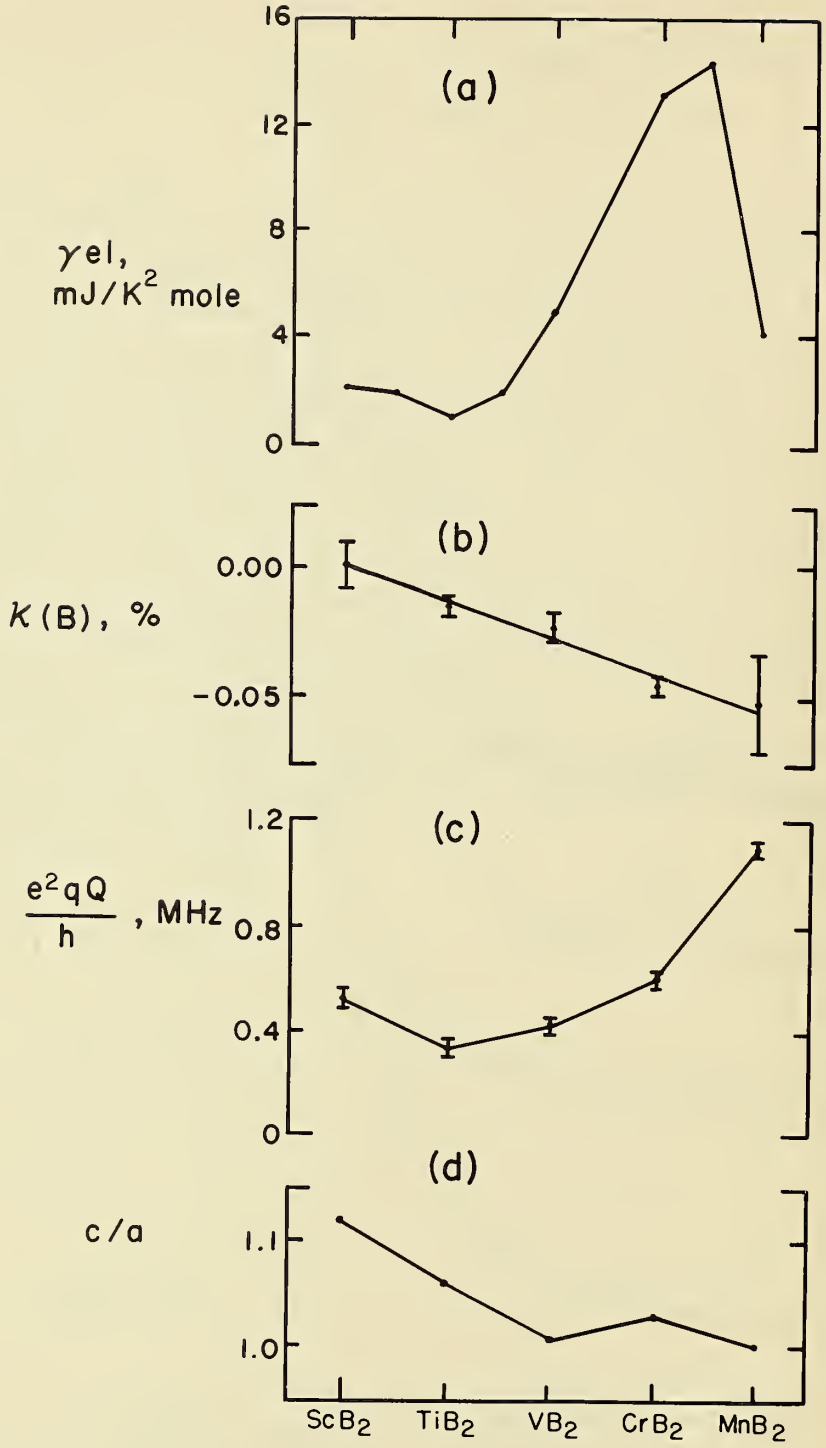

FIGURE 2. Plots of (a) low temperature electronic specific heat, (b) Knight shift of the ^{11}B nuclear magnetic resonance, at room temperature, (c) room temperature first order electric quadrupole coupling constant, and (d) c/a lattice parameter ratio at room temperature for the diborides of the first transition series metals and having the C32 structure.

3.2.3. High Temperature Metals

3.2.3.1. Optical Constants of Titanium

A. J. Melmed and J. J. Carroll
Metallurgy Division
Institute for Materials Research

The objective of this project was to determine the optical constants (complex index of refraction) of titanium by ellipsometry at room temperature in the visible region of the light spectrum. It is recognized that titanium, at room temperature, is optically anisotropic and chemically reactive with the normal atmospheric environment. Therefore measurements in different crystallographic directions, under appropriate clean surface conditions, are necessary for a proper determination of optical constants. In addition it is recognized that considerably more polycrystalline titanium than single-crystal titanium is used outside the laboratory, so that optical constants of polycrystalline specimens were also determined.

Optical constants have been measured at λ = 5461A from a titanium specimen which was prepared in ultra-high vacuum by vapor deposition onto a (011)-oriented tungsten single crystal substrate followed by a low temperature ($\sim$ 500 C) anneal.

The vacuum system used was identical to that which was previously described (1) with the exception of a Ti vapor source located about 1.5 inches from the substrate. Ti vapor was obtained by heating a high purity Ti wire by resistively heating an encircling coil of W wire. The base pressure during these experiments was 1×10^{-9} torr as indicated by corrected cold cathode discharge gage readings, except during part of each Ti evaporation when the pressure rose continuously to about 8×10^{-9} torr.

Prior to Ti specimen preparation the W substrate was characterized as being free from an overlay of an ordered contaminated layer as judged by low-energy-electron diffraction (LEED). A heat treatment

greater than 2000 Å of the W substrate was necessary to generate LEED diffraction pattern display which had no extra ordered diffraction features. At this stage ellipsometry measurements were made in order to furnish the complex index of refraction ($\hat{n}$) of the clean W substrate, where $\hat{n} = n(1-ik)$. Immediately following the above characterization Ti was evaporated in short (2 minutes) and separate doses, each dose being periodic in terms of a constant time interval between equal heat treatments of the Ti evaporator. The as-deposited Ti caused changes in the optical constants n and k of the specimen (substrate and film) as shown in Figure 1.

Successive Ti doses caused n to decrease and k to increase from their respective W substrate values. The LEED pattern generated during Ti depositon showed that the diffraction spots had doubled with an increase in background intensity. Subjecting the specimen to a short low temperature anneal following the 21st dose resulted in little change in the LEED pattern and an expected discontinuous change in n and k. Assuming a film refractive index of that obtained after the 21st dose and anneal on a W substrate having the initially measured optical constants, the Ti average film thickness is calculated as being 348A.

Evidence from parallel experiments using Fe vapor deposition on a similar (011)-oriented W substrate demonstrated that optical constants measured for the annealed film/substrate composite approach bulk Fe values at an Fe film thickness of about 400A (2), due to a lack of a significant contribution to the measured values from the W substrate at or beyond this thickness. Our optical constants data obtained from the above described Ti film experiment, together with the data that Tennyson Smith (3) obtained from bulk (0001)-oriented Ti single crystal cleaned in ultrahigh vacuum by a combination of heating and argon ion bombardment, demonstrate that the same is true for Ti. See Table 1.

Additional measurements of optical constants from bulk (0001)-oriented Ti single crystals were made in air under various conditions using several wavelengths between 3800 and 6000A.

Figures 2 and 3 depict the wavelength dependence of the index of refraction, n, and absorption coefficient, k, of a specimen which was mechanically polished, washed successively in acetone and distilled water, and air dried. The n-spectrum from such a sample closely resembles that of Kirillova and Charikov (4) in both its shape and measured n values. However, the k values obtained from this specimen are about 20% lower than those obtained by these workers - excepting the points at λ = 6000A. Their measurements were carried out in air on Ti specimens which were "polished to the 14th class of finish."

The above mechanically polished specimen was subjected to a chemical polishing treatment, washed in water and air dried. The chemical polishing treatment, which is considered to remove mechanical polishing inclusions and to further smooth the surface, had the effect of increasing n and k values throughout the wavelength span but not changing the shape of either the n or k spectra.

The wavelength dependence of n and k values, obtained by Hass and Bradford (5) from Ti films evaporated at about 10^{-6} torr, is similar in shape to the results obtained from the present work as shown in Figures 2 and 3. However, and in interesting contrast to the data comparison between this work and that of ref. (4), the n values obtained from this specimen are about 20% lower than those obtained by Hass and Bradford (5).

In addition, the observation was made that upon continued exposure to air, the measured values of n and k changed. n values decreased while k values increased in time. It is known that similar changes of n and k take place when (011) W is exposed to either air or oxygen and that these changes from their respective clean surface values occur without disturbing the shape of the n or k spectrum (6).

Although the work of Tennyson Smith (3) is confined to one wavelength, he exercised considerable diligence in determining that the Ti specimen used in the optical constant measurement was free from impurities detectable by Auger spectroscopy.

In view of Smith's work, of the excellent agreement in optical constant determination, and of the effect of contamination upon the apparent optical constants, the n and k spectra can be inferred for the clean (0001) Ti surface condition by parallel vertical shifts of the spectra in their appropriate directions until curve intersection occurs at the correct n and k values for λ = 5461A. The result of such a procedure is shown in Figure 4.

Finally, we note the progression of n values and k values as specimen purity and surface cleanliness is improved, similar to the changes already noted (7) for optical constants of Fe. The situation can readily be seen by inspection of Table 1. In order of improving specimen surface conditions we rank the results as follows: 1)Kirilla and Charikov (1963) and our measurement on mechanically polished (0001) Ti in air; 2) our measurement on chemically polished (0001) Ti in air; 3) Hass and Bradford (1957) on Ti film prepared in vacuum and measured in air; 4) our ultrahigh vacuum Ti film measurement and Tennyson Smith (in progress). As the specimen surface is improved the measured value of n increases and k decreases.

This project has come to its end and this constitutes the final report.

TABLE 1

Titanium Optical Constants

		n	k	λÅ	nk
1.	Ti film (this work)	3.000	1.237	5461	3.711
2.	Tennyson Smith (present)	3.04±0.04	1.234	5461	3.751
3.	Kirillova and Charikov (Bulk Ti polished in air, 1963)	1.85	1.70	5500	3.145
4.	Bulk (0001) Ti (mechanically polished in air, this work)	1.81	1.37	5500	2.480
5.	Hass and Bradford (Ti film exposed to air and corrected for oxide, 1957)	2.53	1.32	5461	3.340
6.	Bulk (0001) Ti (chemically polished in air, this work)	2.05	1.51	5461	3.096

REFERENCES

1. A. J. Melmed, H. P. Layer, and J. Kruger, Surface Science, 9, 476 (1968).
2. A. J. Melmed and J. J. Carroll, Surface Science, 19, 249 (1970).
3. Tennyson Smith, Science Center of North American Rockwell Corporation, Thousand Oaks, California (Private Communication).
4. M. M. Kirillova and B. A. Charikov, Physics of Metals and Metallography (USSR) 15, 138 (1963).
5. Georg Hass and Alan P. Bradford, J. Opt. Soc. Am., 47, 125 (1957)
6. J. J. Carroll and A. J. Melmed, Surface Science, 16, 251 (1969).
7. H. T. Yolken and J. Kruger, J. Opt. Soc. Am., 55, 842 (1965).

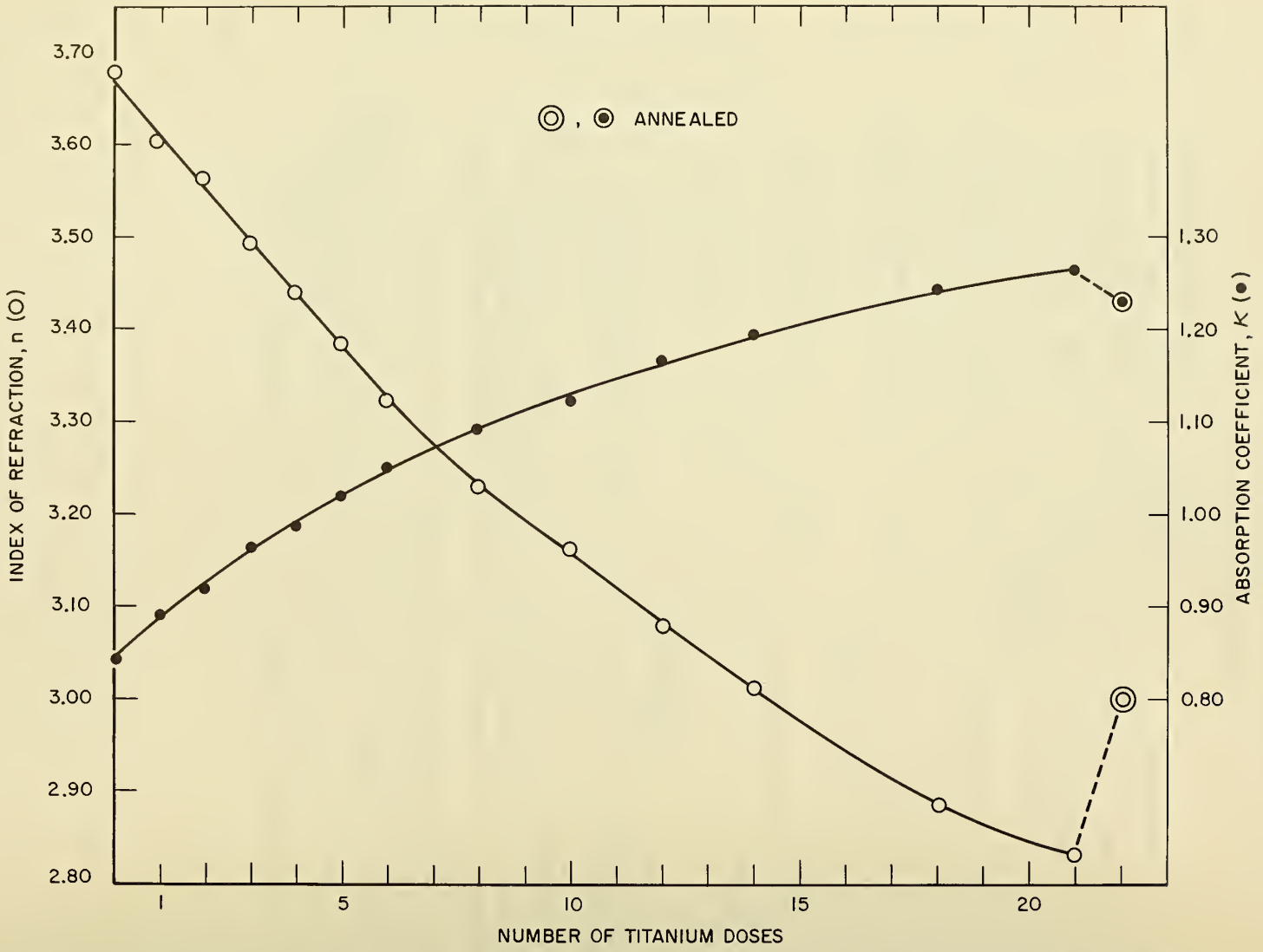

FIGURE 1. Measured index of refraction (n) and absorption coefficient (k) at λ = 5461A as a function of number of Ti doses. The specimen was annealed after dose 21.

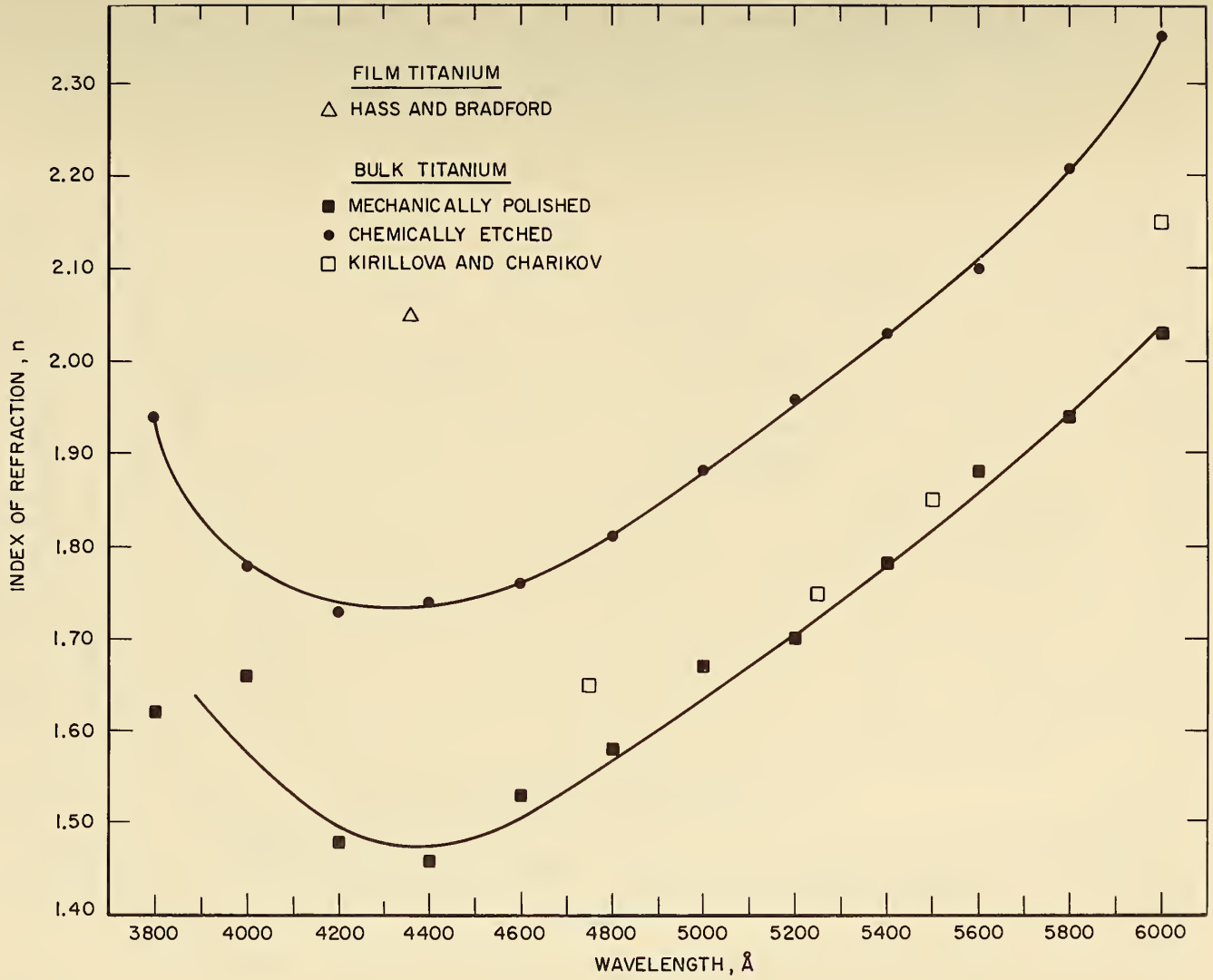

FIGURE 2. The real part, n, of the index of refraction for bulk (0001) Ti in air versus wavelength, λ.

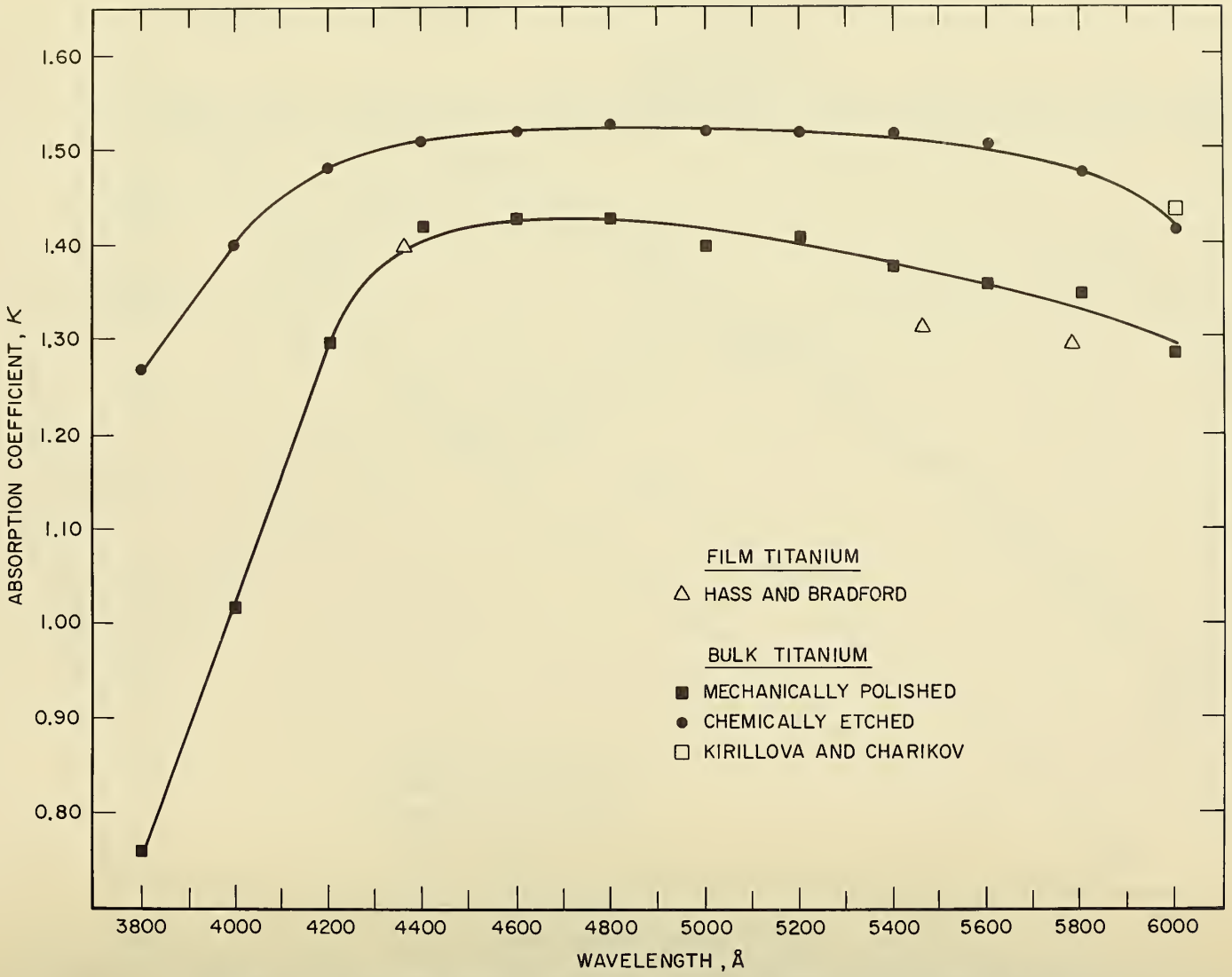

FIGURE 3. The imaginary part, k, of the index of refraction for bulk (0001) Ti in air versus wavelength, λ.

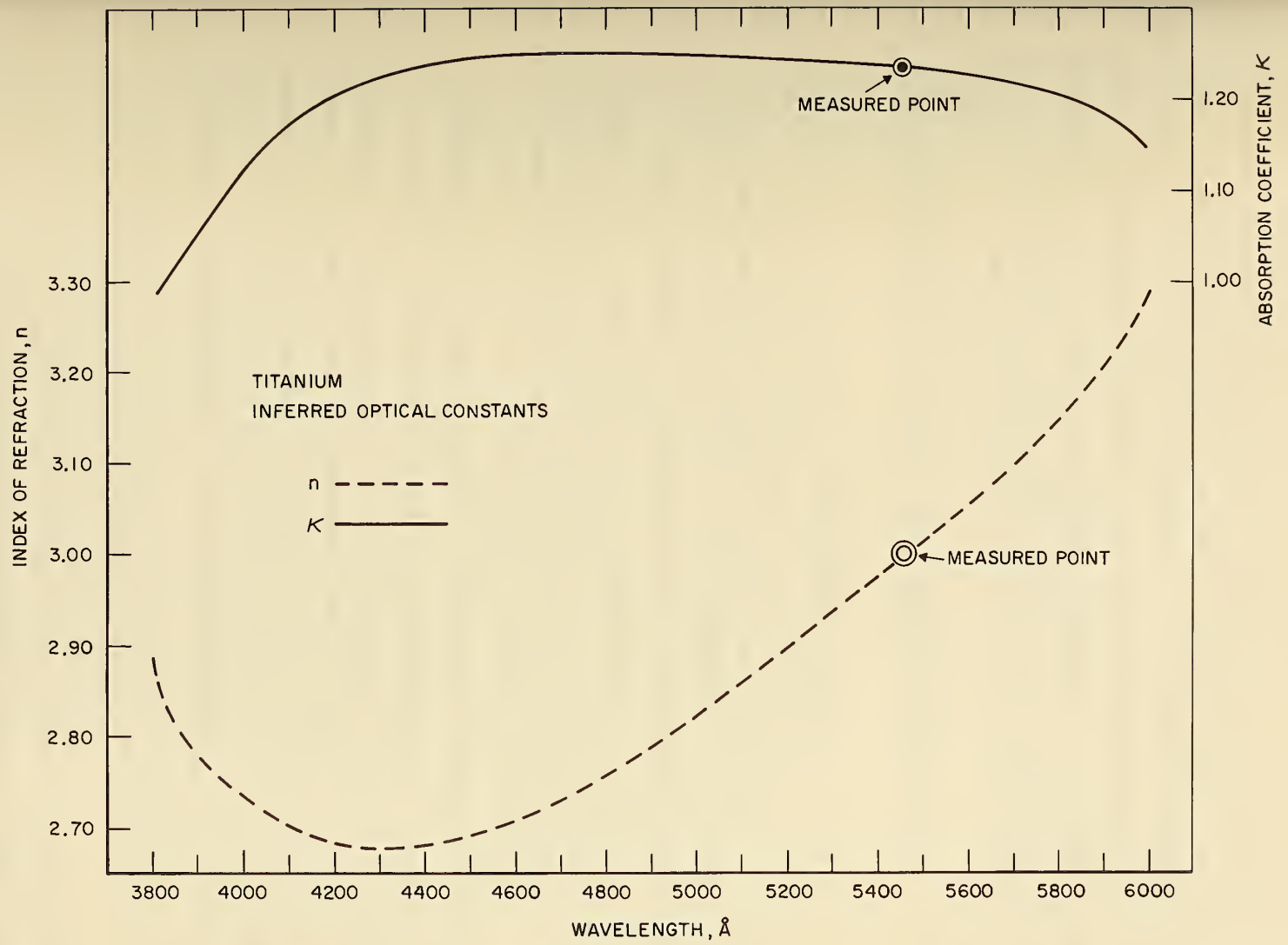

FIGURE 4. Inferred optical constants (n, k) for Ti from the measured values of λ = 5461A versus wavelength, λ.

4. LASER MATERIALS PROGRAM

4.1. Introduction to Laser Materials

The National Bureau of Standards, with support from the Advanced Research Projects Agency (Office of Materials Sciences) of the Department of Defense, is carrying out a program of research on laser materials. This program includes studies to characterize laser materials, to define and evaluate damage measurements in laser materials, and to investigate the degradation of laser performance. A summary of the results achieved during the reporting period is given here.

4.2. Objectives of and Summary of Program in Laser Materials

4.2.1. Objectives

One of the important factors which is limiting the advance of ultra high power laser technology is the failure or degradation of laser materials due to optically induced damage. In the past, the empirical approach to laser materials has been adequate. That is, the damage or degradation to laser materials has been circumvented by equipment design or by a cut-and-try improvement in the laser materials. This problem of optically induced damage now poses a serious threat to the successful application of laser devices to an important class of needs of the Department of Defense. This fact has been recognized and the Advanced Research Projects Agency supports research to improve the performance of laser materials. The convening of three committees to examine the optical damage to laser materials illustrates the present concern and importance of solving this class of problems. These committees are the Subcommittee II of ASTM Committee F-1, the Institute for Defense Analysis studies, and the National Materials Advisory Board Committee on the Fundamentals of Damage in Laser Glass.

The success of these efforts depends upon having the knowledge and proper skills available when they are needed. In the case of laser technology, they include the science and techniques of laser

materials preparation and characterization and of the measurement and evaluation of those properties which are relevant to the damage and degradation of lasers. It is the overall objective of the present NBS program on laser materials to identify some of the more important problems concerning damage and degradation of lasers and to provide the necessary advances in those areas for which NBS possesses the competence to do so. These efforts will be directed mainly toward providing the techniques for the preparation and characterization of laser materials to be used in tests for the measurement and evaluation of material properties pertinent to the damage and degradation of lasers, for the tabulation of key damage data, and for the improvement in the knowledge and skills necessary to advance the performance of lasers.

In pursuit of this program, a continuing attempt is being made to analyze the technological problems associated with high performance lasers and the materials from which they are constructed, and to distill from this analysis major scientific problems whose solutions would advance laser technology. In addition, the problems chosen should fall within areas in which NBS has available competence. Also, the number of problems included in the program should be kept small enough so that each one can be approached in a reasonably comprehensive manner.

In accordance with these criteria, the present program contains three subdivisions - Characterization of Laser Materials, Damage to Laser Materials, and Degradation of Laser Materials. Damage and Degradation as used here are distinguished in that Damage is localized and occurs during the course of a very few pulses whereas Degradation implies the much more gradual and general deterioration of performance over many pulses. There may, of course, be some overlap.

4.2.2. Summary of Progress to Date

4.2.2.1. Characterization of Laser Materials

There is a continuing need for the characterization of laser materials. Suppliers frequently make changes in composition and usually

are not able to provide adequate data on those physical and chemical properties which influence laser performance and the distortion of wave fronts propagating in laser materials. Trace impurities in two ruby laser crystals, grown by a domestic company, have been determined by neutron activation analysis. The elements Cr, Ga, and Ir are distributed in a fairly uniform manner throughout a crystal; Cu and Mn are distributed less uniformly; and the concentrations of Ba and Sr vary greatly from one region to another in a crystal of laser ruby. These crystals also have Ba-rich inclusions which are as large as 20μm in diameter.

The strain-induced birefringence and refractive index variations have been determined for a YAG (yttrium aluminum garnet) rod. Calculations of the strain-induced birefringence in YAG have been made for various crystallographic directions. Although large variations are not found for different orientations, the magnitude of induced birefringence can be reduced by 30 per cent, if YAG boules are grown along the [100] direction. They usually are grown along the [111] direction. A Twyman-Green interferogram of a YAG boule has been made. It shows a pattern having three-fold symmetry due to the strain induced when the crystal is cooled during its growth. The refractive index decreases from the center to the edge of the boule and the maximum variation in the refractive index is 2×10^{-5}

4.2.2.2. Damage to Laser Materials

Inclusion damage (bulk) has been a serious source of difficulty for the laser systems engineer concerned with ultra-high power pulses. Although surface damage and intrinsic damage (self-focusing or beam trapping) contribute additional problems, these are at present apparently not as great an obstacle to the advance of laser technology as is the inclusion damage. A laser glass damage test facility is being constructed at NBS to study the damage problem and to attempt to bring some unity to the great proliferation of damage data. This test facility will center around a one gigawatt neodymium glass laser system

and will be used to develop standards for performing meaningful (reproducible) measurements on the damage mechanisms which are produced by high energy laser pulses. The construction of this facility includes detailed characterization of the laser beam. Near field intensity profiles of this laser have been made and have been compared with other neodymium lasers. These profiles will be used as a guide to make certain that the NBS laser has a reasonably homogeneous beam. The necessity for having a homogeneous beam in order to obtain meaningful damage measurements has been stressed at several conferences.

A theoretical model for studying the thermal stresses produced by inclusions in laser materials has been developed. The thermal stress which is thought to cause fracture in laser glasses is the tangential-tensile stress near heated inclusions. The model has been used to study three questions. First, how the maximum tangential-tensile stress varies as a function of the radius of the spherical inclusion for a fixed energy density and pulse width of the laser beam. Second, how the maximum of the tangential-tensile stress varies as a function of the thermal conductivity and the thermal expansion coefficient of the host. And third, if the maximum temperature of the inclusion is limited to a fixed value, how the parameters of a laser beam should be varied to increase the probability of detecting by optical techniques a small incipient absorbing center before it causes damage. Two important conclusions predicted by this model are that submicron-sized inclusions have the greatest probability to cause damage in laser glass hosts and that the lens effect arising from heated inclusions probably does not cause damage.

4.2.2.3. Degradation of Laser Materials

At present, the degradation of some ruby and YAG laser rods after continued use is not well understood. The reasons are in part a lack of sufficient data on the differences among coloration by laser pump light, x-ray irradiation, and γ-ray irradiation. The electron

paramagnetic resonance (the EPR, $\Delta m = 2$ transition) in γ-ray irradiated (^{60}Co) ruby and the optical absorption of x-ray irradiated ruby have been measured as a function of the Cr concentration. The respective results have been compared with one another. The comparison does not permit us to make at present definite-positive models of the observed color centers. The Cr concentration dependences of the EPR spectra in γ-irradiated ruby and of the optical absorption in x-ray irradiated ruby suggest that the respective centers may have a mechanism in common. The coloration of x-ray irradiated ruby is too intense to be explained by valence changes of the Cr ions because the required oscillator strength would be unreasonably large. Thus, the coloration is thought to arise from another, as yet unspecified, color center. The center produced by γ-ray irradiation could be related to, but does not arise necessarily from the same center.

Independent evidence suggests that the concentration of the Cr^{3+} ion plays an important role in the coloration process. Thus, techniques for determining the Cr^{3+} ion concentration in several ruby samples have been considered. Activation analysis does not provide information on the valence states of the ions. Three promising techniques, examined thus far, include measuring the intensities of EPR lines, the magnetic susceptibility due to Cr^{3+} ions, and the absorption coefficients at the band maxima for the Cr^{3+} ions. Theories are used then to relate these measurements to the Cr^{3+} concentrations.

4.3. Project Summaries in Laser Materials

4.3.1. Characterization of Laser Materials

4.3.1.1. Physical and Chemical Properties of Laser Materials

G. W. Cleek and R. M. Waxler
Inorganic Materials Division
Institute for Materials Research

This project was established to determine the physical properties of laser glasses and crystals and to relate these properties to their chemical composition.

Accomplishments

Measurements on five commercially-made Nd-doped laser glasses and single crystal ruby have been completed. Data were obtained on refractive index, thermal change in refractive index, elastic constants, photo-elastic constants, thermal expansion, density and chemical composition. These data are needed to calculate the corrections for the thermal distortion of the wavefront in light generated by laser rods.

Results of the study on the photo-elastic properties of single crystal ruby have been published(‡). Data on the refractive properties of Nd-doped laser glasses are being prepared for publication.

During the current reporting period, neutron activation analyses have been completed on ruby samples, examinations of a YAG boule were made to determine its optical quality by shadowgraph and interferometric methods, and theoretical calculations of the photo-elastic properties of YAG have been made.

Chemical Analyses*

Ruby Specimens - Neutron activation analysis was used for the determination of trace impurities in specimens from two ruby laser crystals grown by a domestic company. The specimens as received were cut from ruby boules and had circular cross sections about 2 mm thick. Each specimen was then cut into four quarters. Each quarter weighed about one gram. Two pieces from each boule were sealed in polyethylene and irradiated for 60 minutes in pneumatic tube RT-4 of the National Bureau of Standards Reactor at a power level of 10 MW (1×10^{13} n.cm^{-2} sec^{-1}). A Cu flux monitor was taped to the outside of the polyethylene to permit normalization of small differences. After irradiation the samples were rinsed in acetone and 1:1HNO_3 to remove surface contamination. Their gamma spectra were

* Neutron activation analyses were performed by Barbara A. Thompson, Analytical Chemistry Division.

Figure 1. Twyman-Green interferogram of YAG boule.

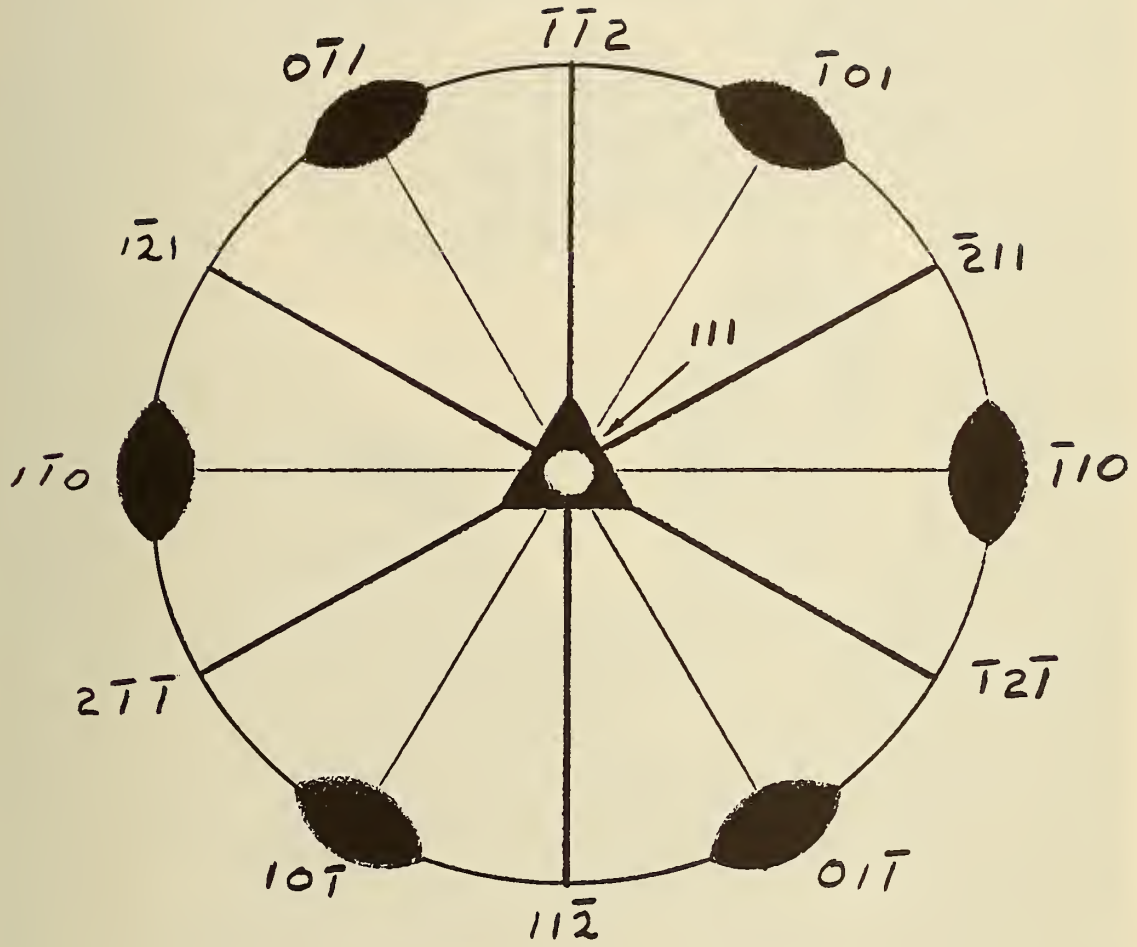

Figure 2. Stereogram showing the symmetry elements of the (111) plane in a YAG crystal.

Figure 3. Birefringence pattern of the YAG boule place between circular polarizers.

measured with a 47-cc Ge(Li) detector and a 2048 channel analyser. Concentration levels were determined for the elements observed by comparison to standards.

The results obtained are shown in Table I. All results are in ppm of the element except for Cr, which is reported in per cent Cr_2O_3. As was found in previous analyses, Cr, Ga, and Ir appear to be fairly uniformly distributed within a crystal; Cu and Mn are less uniform and Ba and Sr fluctuate wildly. Further examination by the optical microscope revealed small particles, which were up to 20 μm in diameter, embedded in the crystal. Examination by the x-ray microprobe indicated that these were rich in Ba. The origin of these Ba-rich inclusions in ruby crystal is not known.

TABLE I

Results of Activation Analysis of Ruby Crystals, ppm

Element	Crystal Designation, Boule No. 2 - 387 - 4		4 - 546 - 2	
	A	B	A	B
Cr (%Cr_2O_3)	0.0373	0.0351	0.0389	0.0377
Ir	0.045	0.041	0.052	0.051
Ga	0.008	<0.006	0.030	0.031
Mn	0.0008	0.0006	0.0009	0.0056
Cu	0.024	0.016	0.027	0.137
Ba	0.28	1.74	16.5	265.
Sr	<0.03	0.085	0.54	8.3

Studies on YAG

YAG (yttrium aluminum garnet) has proved to be one of the most versatile crystalline host materials for solid lasers. An undoped boule of YAG, 12,6 cm x 2.0cm dia. was grown by a domestic company and shipped to NBS for photoelastic studies. The growth direction in this boule is colinear with [111] and its threefold symmetry is expressed by six (211) facets. This crystal was grown by the Czochralski method, and the melt was established in an iridium

crucible containing a stoichiometric batch of single crystal alumina crackle and yttrium oxide powder.

It has been found that one of the problems encountered in firing a YAG laser is the thermal distortion introduced into the laser cavity by the deposition of heat from the flash lamps (2). Because a thermal gradient is established from the center to the edge of the rod, there is a distortion of the wavefront of the light generated which arises from the temperature-induced changes in refractive index.

In addition, the temperature gradient creates internal stresses which produce further changes in index induced by the stress-optic effect. Since YAG is a cubic crystal and is optically isotropic, the change in refractive index with temperature is independent of crystallographic direction. Internal stresses, however, cause the crystal to become anisotropic, so that an optimum optical element could be one selected on the basis of the crystal photoelastic constants. Until now, the direction [111] has been accepted as the standard YAG growth and lasing direction without justification other than that crystals with that orientation are available (2).

Dixon(3) has reported that the elasto-optic constants of YAG are

$$p_{11} = -0.029$$
$$p_{12} = +.0091$$
$$p_{44} = -.0615*.$$

---

* From these data, using the relationship $q_{ij} = \sum_{1}^{6} p_{ik} s_{kj}$, the piezo-optic constants were calculated to be

$$q_{11} = -.0121 \times 10^{-12} \text{ m}^2/\text{N}$$
$$q_{12} = +.051 \times 10^{-12} \text{ m}^2/\text{N}$$
$$q_{44} = -.535 \times 10^{-12} \text{ m}^2/\text{N}$$

The s_{kj} represent elastic compliances. Values have been reported by Spencer, El.al.(4).

On the basis of these data, calculations have been made of the strain-induced birefringence in YAG for various crystallographic directions. The results are shown in Table II where it can be seen that growth along [100] is the most favorable direction. Although large variations are not found for the different orientations, if boules are grown along [100] instead of [111] as they are at present, the magnitude of induced birefringence can be reduced by about 30 per cent.

The equations and background for the calculations can be found in a paper by Bhagavantam(5). Because YAG is a cubic crystal, the thermal conductivity and thermal expansion are independent of crystallographic direction. It follows then, that for a given temperature distribution in a specimen of YAG, the magnitude of induced strain is independent of direction while the magnitude of induced stress is not(6). Accordingly, the calculations have been made on the basis of constant strain.

Apart from the induced birefringence, it is important to minimize the absolute changes that are induced by strain. Dixon(3) has pointed out that in YAG the elasto-optic constant, p_{12}, is anomalously small. This is desirable for a laser host. The elasto-optic constant, p_{11}, is also small. The largest of the elasto-optic constants is p_{44}. Calculations have not yet been made, but it is apparent that growth along [100] is the best direction for minimizing absolute changes in refractive index. Along [100] the large contribution of p_{44} to refractive index is eliminated, and only the small contributions of p_{11} and p_{12} remain.

The ends of the YAG boule were ground and polished so that they were flat and parallel. The He-Ne laser radiation of 632.8 nm was used to produce a Twyman-Green interferogram of the boule. The picture is shown in Figure 1. This test affords a measure of the variations in optical thickness; in the pattern shown, the fringes are lines of iso-optical thickness spaced at one half wavelength. Calculations showed that the maximum variation in refractive index was 2×10^{-5}. The refractive index decreases from the center to the edge of the boule. The

poor resolution of the fringes in the center of the picture is due to an optical inhomogeneity, known as the core, which runs the length of the boule. The core is a problem peculiar to Czochralski growth. It measures in this boule about 2 mm in diameter. Laser rods are cut from regions which exclude the core.

In Czochralski-grown crystals, variations in refractive index are caused primarily by strain and variations in impurity level. From the symmetry of the pattern, it may be inferred that strain has been introduced during the cooling of the crystal. This is similar to the strain patterns which exist in glass that has not been well annealed.

It is possible to account qualitatively for the three-fold pattern of Figure 1 by using general symmetry principles. YAG is a cubic crystal belonging to the O_h class. A stereogram showing the symmetry elements of the (111) plane is shown in Figure 2. The open triangle represents a $\bar{3}$ axis, the diad symbols represents 2-fold axis, and the heavy lines indicate mirror planes. When the YAG boule became strained during cooling, the strain pattern was independent of crystallographic direction because the thermal conductivity and thermal expansion are isotropic. The strains, therefore, will be essentially radial and tangential(6). The magnitude of the induced stresses will vary from point to point. Furthermore, these stresses will, in general, make the refractive index ellipsoid become triaxial, and the principal axes of the stress ellipsoid and the refractive index ellipsoid will not coincide in the general case. However a uniaxial stress which exists along certain preferred directions of symmetry, i.e. parallel or perpendicular to one of the three mirror planes will constrain two of the principal refractive indices to lie in the mirror plane. Therefore, maxima or minima of the refractive index ellipsoid can be expected to lie along or perpendicular to the trace of a mirror plane.

Laue back-reflection x-ray techniques make it possible to associate directions in the strain pattern of Figure 1 with crystallographic directions shown in Figure 2. The small circles shown in the margin

of Figure 1 correspond to the directions $[2\bar{1}\bar{1}]$, $[\bar{1}\bar{1}2]$ and $[\bar{1}2\bar{1}]$.

A pattern of birefringence was obtained by placing the boule between circular polarizers. This technique makes it possible to ascertain the magnitude of the birefringence regardless of the orientation. Using the sensitive red tint plate and color chart indicates that the optical path difference excluding the core was 250 nm. A photograph of the pattern is shown in Figure 3. This figure also exhibits a three-fold symmetry. The crystallographic directions $[2\bar{1}\bar{1}]$, $[\bar{1}\bar{1}2]$ and $[\bar{1}2\bar{1}]$ are indicated by the small circles in the margin.

REFERENCES

1. R. M. Waxler and E. N. Farabaugh, J. Res. NBS 74A,[2] 215 (1970).
2. D. E. Witter, Union Carbide Corporation, private communication.
3. R. W. Dixon, J. Appl. Phys. 38 5149 (1967).
4. E. G. Spencer, et.al., J. Appl. Phys. 34 3059 (1963).
5. S. Bhagavantam, Proc. Indian Acad. Sci. A37 585 (1953).
6. L. H. Adams and R. M. Waxler, Temperature-Induced Stresses in Solids of Elementary Shape, NBS Monograph 2 (1960).

TABLE II

Calculations of the Birefringence

Induced in YAG by Strain*

Direction of Strain	Direction of Observation	Birefringence nanometers per cm
[001]	[100]	7.1
[001]	[010]	7.1
[100]	[001]	7.1
[100]	[010]	7.1
[010]	[100]	7.1
[010]	[001]	7.1
[001]	[110]	7.1
[001]	$[\bar{1}10]$	7.1
[110]	[001]	11.5
[110]	$[\bar{1}10]$	9.3
$[\bar{1}10]$	[001]	11.5
$[\bar{1}10]$	[110]	9.3
[111]	$[\bar{2}11]$	11.4
[111]	$[01\bar{1}]$	11.4
$[\bar{2}11]$	[111]	10.0
$[\bar{2}11]$	$[01\bar{1}]$	10.9
$[01\bar{1}]$	$[\bar{2}11]$	10.7
$[01\bar{1}]$	[111]	10.0

* All calculations have been based on the strain, $d\ell/\ell = 62.0 \times 10^{-7}$. This strain is calculated to produce a birefringence of 10 nanometers/centimeter when the strain is along $[\bar{2}11]$ and observation is along [111]. This latter figure has been selected as a basis for comparing the magnitudes of birefringence according to the various directions of strain and observation.

4.3.2. Damage to Laser Materials

4.3.2.1. Laser-Induced Damage Studies

Albert Feldman, Roy Waxler and Deane Horowitz
Inorganic Materials Division
Institute for Materials Research

Objective

The objective of this work is the development of a laser test facility to determine damage threshold parameters of laser glasses used in pulsed-high energy laser systems and to establish the diagnostic procedures for identifying the dominant mechanisms of damage. To achieve this objective, methods first must be developed for measuring the laser beam characteristics.

Although damage test facilities exist at industrial laboratories, it is desirable for the Federal Government to have its own laser test facilities in which impartial tests can be performed. Present planning indicates that the National Bureau of Standards will have the only Government laser test facility available for laser glass testing on a full-time basis (1).

Technical Approach

There are three types of damage caused by high energy pulses in laser glass; intrinsic bulk damage, surface damage, and bulk damage due to inclusions. At the present time, the damage threshold data has a large scatter. From the literature one cannot determine whether the scatter is due to sample variation or to variation of the test laser beam parameters. Hence, in order to obtain reproducible and meaningful damage threshold data, it is necessary to have a laser beam with well defined beam characteristics (2). These beam characteristics are listed below:

1. Total energy contained in the laser beam.

2. Cross-sectional energy distribution in the beam for the near and far fields (beam profile).
3. Total power contained in the laser beam.
4. Time evolution of the beam intensity.
5. Frequency spectrum of the laser beam.
6. Time evolution of the frequency spectrum of the laser beam.
7. Reproducibility of the above beam characteristics.

The capability for measuring all these beam characteristics on our laser system must be developed first. The laser system then must be modified to produce a laser beam with the optimum beam characteristics for reproducible and meaningful measurements. At present, it appears most important to have a beam with a uniform cross-sectional energy distribution. Thus, the emphasis in this report is on measurement of beam profile.

Laser System

During this report period acceptance tests were being performed on a commercial neodymium-doped glass laser system. The laser system is depicted schematically in Figure 1 with nominal parameters listed. It consists of an oscillator and two amplifiers, and is Q-switched by means of a Pockels cell. The oscillator rod is 1/2 inch (1.27 cm) in diameter by 6 inches (15.2 cm) long with flat ends. It is apertured down to 1/4 inch (0.635 cm) diameter. A three-power beam expander stands between the oscillator and the amplifier rods. The first amplifier rod is 3/4 inch (1.91 cm) in diameter by 11 inches (27.9 cm) long. The entrance face is flat and the exit face has a Brewster window. Both ends of the second amplifier are cut at the Brewster angle. The output from the laser has been measured at 32.8 J with a pulse width of 18 ns.

Consultations

Consultations were held with John McMahon of the Naval Research Laboratory, Henry Dardy of Catholic University, Harold Boyne, Donald Jennings and Richard Smith of NBS (Boulder) and Merritt Birky of NBS (Washington, D.C.). Methods for measuring laser beam characteristics were discussed. These conversations corroborated our own conclusion that a well defined uniform beam is of prime importance for obtaining reproducible damage threshold data. This conclusion was further confirmed by discussions at the American Society for Testing Materials (ASTM) Symposium on Laser-Induced Damage held in Boulder, Colorado, June 23 to 25, 1970.

The ASTM is currently writing proposals to standardize measurements of beam profile.

Beam Uniformity

Two basic methods, which we will attempt to use, were proposed by the ASTM.

The first method developed by Merritt Birky(3) involves photographing the multiple images of a laser beam as it undergoes successive reflection in a tilted glass plate. The beam becomes progressively attenuated at each reflection. The photographic plate thus simultaneously records the beam at different intensity levels.

The second method involves photographing the diffuse image of the laser beam that impinges on a MgO diffuser. The image is photographed with a multiple lens camera. Behind each lens is a different neutral density filter. Thus, the multiple images on the photographic plate record different levels of intensity. A camera to do this is available commercially.

A major difficulty when using these methods with the 1.06 mm radiation of a neodymium glass laser system is the photographic plates.

At present the only emulsion available is a Kodak Type IZ (4). This film is difficult to handle in that it must be hypersensitized in most uses, and it must be stored in a freezer (4).

A difficulty with the second method occurs because the MgO diffuser, which is made from compressed MgO powder, can disintegrate when hit by a laser pulse.

Estimates of beam uniformity can also be obtained from burn patterns. One method involves subjecting exposed polaroid film to a laser pulse. John McMahon has obtained beam profile measurements on his laser by taking far field burn patterns on a calibrated French photocopy paper while successively interposing different neutral density filters. This method can be used only if the laser beam characteristics are reproducible from pulse to pulse. Nicholas N. Winogradoff in our laboratory has developed a method for obtaining high contrast burn patterns. This method involves exposing Schott NG1 glass neutral density filters to the laser beam.

Future Activities

Our present concern is to measure the laser beam characteristics. We shall attempt to obtain single transverse mode lasing action. This will yield a Gaussian beam profile. We shall accomplish this by decreasing the aperture on the oscillator rod. Although the resulting energy output will be much less than 30 J, we expect no difficulty in producing glass damage because we intend to use a focused beam configuration. With this system we intend to establish test procedures for measuring thresholds of bulk damage in laser glasses.

REFERENCES

1. The Naval Research Laboratory has a glass damage testing program but its laser is available for such purposes only on a part-time basis. We refer the reader to the National Materials Advisory Board Report on the Fundamentals of Damage in Laser Glass,

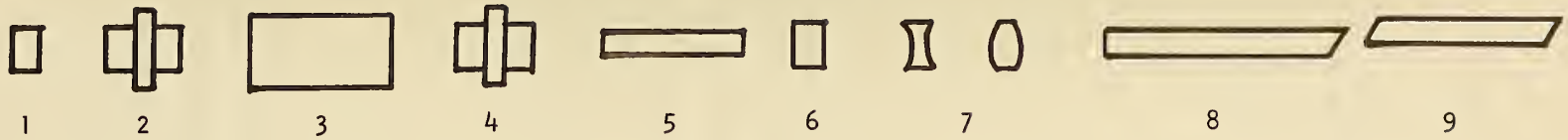

1. Back mirror 100% reflecting.
2. Tent polarizer vertical polarization.
3. Pockels' cell.
4. Tent polarizer horizontal polarization.
5. Oscillator rod 15 x 1.3 cm 3J output.
6. Front mirror - sapphire etalon which in combination with front surface of oscillator rod gives 38% reflectance.
7. Beam expander 3X.
8. Preamplifier rod 28 x 1.9 cm, one Brewster end 57°, 18J output.
9. Final amplifier rod 18 x 1.9 cm, two Brewster ends 57°, 30J output.

FIGURE 1. Schematic representation of the laser system.

Publication NMAB - 271 (July 1970), National Academy of Science-National Academy of Engineering, Chapter XI.
2. H. G. Heard, Laser Parameter Measurements Handbook, (John Wiley and Sons, Inc., New York, 1968).
3. Merritt M. Birky, Applied Optics 8, 2249 (1969).
4. Kodak Plates and Films for Science and Industry, Kodak Publication No. P-9, p. 20, 25.

4.3.2.2. Inclusions in Laser Materials

Herbert S. Bennett
Inorganic Materials Division
Institute for Materials Research

Objective

One of the severe problems encountered in high-power-solid-state laser systems is the thermal damage to laser rods and optical elements. One such type of damage is thought to arise from metallic or dielectric inclusions. Such inclusions may absorb an appreciable amount of incident laser radiation and thereby may undergo thermal expansion. This produces major stresses within the host material. The objective for this report period was to solve the heat diffusion equation and the thermal stress equations in order to estimate such thermal properties of the absorbing center-host system.

Summary

The optical path length change for a probing light ray passing near the absorbing center, the radial and tangential stress components, and the changes of the refractive index for radially polarized and tangentially polarized light due to the thermal stress field were computed. The dependence of the maximum value of the tensile stress

---

* An associated project, supported by the National Bureau of Standards.

upon the size of the inclusion and upon the physical properties of the of the host was examined. The feasibility of using optical techniques to detect metallic and dielectric inclusions in laser materials before they cause damage also was studied. These computations suggest that the use of laser pulse widths of the order of microseconds or longer may be more promising for the detection of small incipient absorbing centers than the use of nanosecond pulse widths. In addition, the lens effect was estimated.

Approach

The results to be summarized in this report are based upon a linear theory and upon a model whose elastic, thermal, and optical properties are constants. The values for these properties are valid for temperatures near 300 K and for small strains. This treatment is not expected to be correct near the onset of damage. The problem is certainly a nonlinear one near the region of catastrophic damage. Whenever any of the assumptions become invalid, then the results should be viewed as suggesting trends in the behavior of the system. The inclusions which occur in laser glasses are most likely not the spheres for which the model has been formulated. They could be irregularly shaped globules. Some platinum inclusions occur as hexagonal platelets. Even though the model does not take into account such geometrical aspects, one hopes that it does give a reasonable description of the actual system. One also hopes that the manner in which it suggests one should proceed to increase the damage threshold, though probably not quantitatively correct, is qualitatively correct.

A model to represent the behavior of absorbing centers in laser materials is developed. Before the thermal properties of the absorbing center-host system can be discussed quantitatively, it is first necessary to solve the time-dependent heat diffusion equation for the temperature and the thermal stress equations with appropriate boundary conditions for the stress components. This is discussed in detail in Ref. 1 and Ref. 2. Reference 1 is given in the appendix to this report.

The model contains many physical assumptions which are necessary to render the problem solvable. The major assumptions are summarized here and also are discussed in greater detail in Ref. 1 and Ref. 2.

a) The inclusion is a sphere of radius r_o and is always in good thermal contact with the host. The effects of shape and orientation to the incident radiation are thus neglected.

b) The host material is isotropic, continuous and of infinite extent. It also is initially at an ambient temperature T_o and free from all stresses and strains. Because the energy content of the incident radiation is finite, the latter statement requires the temperature to be T_o at infinity and all stresses and strains to vanish at infinity. The distribution and nature of microcracks and optical imperfections are not treated in the model.

c) The linear-thermal-elastic equations are assumed to give a reasonable description of the processes which ultimately may lead to catastrophic damage. These equations are coupled equations relating the temperature and the displacement vector from which the stresses and strains are computed. They are valid only when a local temperature exists and when distances are larger than atomic dimensions ($\sim 10^{-8}$cm). A relaxation time t_r for the definition of a local temperature T is approximately the reciprocal of a characteristic vibration frequency of the material. These relaxation times t_r for Pt, Sb, Al_2O_3, and the laser glasses are about 10^{-13}s to 10^{-12}s. Hence, the equations are physically meaningful when times t are much larger than 10^{-12}s.

d) It is assumed that the radiation of heat by the center-host interface and by the heated glass close to the absorbing center may be neglected in the thermal-elastic equations. The laser beams studied in Ref. 1 and Ref. 2 contain energy fluxes at least 10^4 times greater than the energy flux produced by a black body at 600°C. The calculations of Ref. 1 also show that the energy flux due to thermal conduction greatly exceeds the energy flux due to radiation for times less than one second. Because the temperature is close to the ambient temperature whenever the pulse width of the

laser beam is greater than a second, the long time behavior is not in the region of practical interest for detecting incipient damage centers before they cause damage. Hence, it is assumed that all times are less than a second.

e) The linear-thermal-elastic equations contain a coupling term and an inertia term. These two terms may be neglected whenever the three characteristic times which occur in the absorbing center-host system satisfy a set of inequalities. These times are the following. The pulse width τ of the incident radiation determines in part the rapidity of heat generation. The characteristic relaxation time for temperature equilibration (thermal diffusion) is $t_T \sim (r^2/a^2)$, where r is the radial distance from the center of the inclusion and a^2 is the thermal diffusivity. The characteristic mechanical time required for the production of stress waves is $t_M \sim (r/v)$, where v is the speed of propagation of elastic waves. Boley and Wiener have demonstrated that when $\tau >> t_M$ and $t_T >> t_M$, then the coupling and inertia terms are small compared to the other terms in the equations(3). The above inequalities are reduced to inequalities containing the pulse width τ and the radial distance r(1); namely:

$$\tau >> 2.8\text{x}10^{-6}\text{(s/cm) r and r} >> 6.7\text{x}10^{-7}\text{cm.}$$

It is assumed that these inequalities are satisfied and thereby that the coupling and inertia terms may be neglected.

In summary, the following inequalities describe the regions for which the model is physically meaningful:

$$10^{-3}\text{s} > \tau > 10^{-12}\text{s},\ 1\text{s} > t > 10^{-12}\text{s},$$
$$r > 6.7\text{x}10^{-7}\text{cm, and } \tau > 2.8\text{x}10^{-6}\text{(s/cm) r.}$$

Results:

The numerical results which the model developed in Ref. 1 predicts are summarized here. Among the many input parameters, the absorptance $A(\lambda,T)$ of the center-host interface is perhaps most sensitive to the initial thermal contact and surface conditions of the inclusion and

host. The wavelength is λ. The numerical results are given for the case in which $A(\lambda,T) = 1$. This presents no additional problem because the temperature $T_h(r,t)$, the optical path length change ΔL for a probing light ray passing near the inclusion, the stress components σ_{rr} and $\sigma_{\theta\theta} = \sigma_{\varphi\varphi}$ for the spherical coordinates r, θ, and φ, and the changes in the refractive index due to the thermal stress field for radially polarized light Δn_r and for tangentially polarized light Δn_θ are all directly proportional to the absorptance.

The model has been used to study three questions. First, how the maximum tangential-tensile stress varies as a function of the radius of the spherical inclusion for a fixed energy density E_L and pulse width of the laser beam τ. Second, how the maximum of the tangential-tensile stress varies as a function of the thermal conductivity and the thermal expansion coefficient of the host. And third, if the maximum temperature of the inclusion is limited to a fixed value, $T_h(r_o,\tau) = 600°C$, how the parameters of the incident laser beam should be varied to increase the probability of detecting by optical techniques a small incipient absorbing center before it causes damage. Optical techniques to detect small inclusions become more promising, the greater ΔL, Δn_r, and Δn_θ are.

The bulk thermal, elastic, and optical properties for the laser material used in these calculations are representative of two Nd-doped laser glasses manufactured domestically. The inclusions are Pt, Sb, and polycrystalline Al_2O_3 absorbing spheres.

The variation of the maximum tensile stress $\sigma_{\varphi\varphi}$ (max-tensile) as a function of r_o for a laser beam having an energy density $E_L = 20$ (J/cm^2) and a pulse width $\tau = 30$ns is studied. When 10^{-4} cm $> r_o > 5\times10^{-5}$cm, the maximum tensile stress exceeds by as much as a factor of two the theoretical strength of the glass (6×10^9N/m^2). The calculations show that Sb and highly absorbing Al_2O_3 inclusions are more

likely to cause damage than Pt. The maximum tensile stresses for Sb and Al_2O_3 inclusions are about 20% larger than those for Pt. It is interesting to note that one domestic manufacturer no longer uses Sb_2O_3 as a fining agent.

These results demonstrate that submicron-sized inclusions have the greatest probability to cause damage in laser glass hosts. Experimental measurements performed by industrial researchers have verified tentatively this theoretical result. Very large ($r_o > 10^{-4}$ cm) and very small ($r_o < 5\times10^{-5}$ cm) inclusions are not likely to produce damage.

The maximum tensile stress as a function of the thermal conductivity K_h and the thermal expansion coefficient α_h is also studied for

$$r_o = 5\times10^{-5}\text{cm},\ \tau = 30_{\mu s},\ \text{and}\ E_L = 20\ (\text{J/cm}^2)$$

It is found that increasing K_h from 0.008 (W/cm°C) to 0.04 (W/cm°C) with all remaining properties kept constant decreases the maximum tensile stress from about 9×10^9 (N/m^2) to 4×10^9 (N/m^2). Again, all the other properties of the host are kept the same except for the thermal expansion coefficient. The maximum tensile stress is studied then as a function of α_h. The maximum tensile stresses are found to have minimum values for

$$10\times10^{-6}\ °C^{-1} > \alpha_h > 8\times10^{-6}\ °C^{-1}$$

Values of α_h outside this range yield larger stresses. They also are slowly varying functions of the thermal expansion coefficient. Increasing α_h by a factor of three produces only a 10% variation in the maximum tensile stress. Hence, the thermal conductivity influences greatly the behavior near the region of maximum tensile stress and the thermal expansion coefficient plays only a minor role in the value of the maximum tensile stress. Among the many possible glass laser hosts, the expansion coefficients vary by about an order of magnitude from $10^{-6}\ °C^{-1}$ to about $10\times10^{-6}\ °C^{-1}$ and all the remaining bulk elastic and thermal properties vary by only small amounts. The latter variations usually do not exceed a factor of two. Hence, extensive research

on altering substantially the composition of present laser glasses to increase the damage threshold due to inclusions is not warranted by the predictions of this model. It suggests that probably at the best, a factor of two increase in the damage threshold could be achieved. This suggestion agrees with one of the conclusions of the National Materials Advisory Board Committee on the Fundamentsls of Damage in Laser Glass.

The model also shows that the maximum value for the tensile stress does not depend upon the Young's modulus E in a straightforward manner as some reseachers have suggested. The Lamè constants are the independent elasticity variables and changes should be discussed in terms of them. If it were possible to alter only the Young's modulus, then the stresses would increase in a monotonic fashion with increasing values of E. But such changes are not possible in practice. The model predicts that glasses with higher E values are not necessarily more resistant to damage.

The optimum parameters of the incident laser beam to be used for detecting incipient damage centers before they cause damage are examined for the case in which the maximum temperature is 600°C at the cessation of the laser pulse. The computations indicate that pulse widths of the order of microseconds or longer heat the center more slowly and thereby produce larger optical path length changes for a probing light ray passing near the inclusion. For example, a Pt sphere with radius $r_o = 10^{-4}$cm produces a path length change of about 2×10^{-8} cm for $\tau = 0.1\mu s$ and of about 10^{-6} cm for $\tau = 100\mu s$. Researchers (American Optical Company) using microsecond pulses and holography have detected 5×10^{-3} cm inclusions without causing damage. It is not known yet whether this method can be improved sufficiently to detect 10^{-4} cm inclusions.

Finally, the lens effect due to heated regions of the host is estimated. Whenever the refractive index increases with temperature, $(dn_h / dT_h) > 0$, and even though the inclusion does not produce damage at its site, the heated region of the host surrounding the inclusion might focus the same laser pulse or a succeeding laser pulse which

occurs after sufficiently short times and before the heated region cools. The lens effect is estimated by considering the focal length f of a spherical lens having a radius r and mean refractive index n_1. The refractive index of the host is n_h and because $(dn_h/dT_h) > 0$, $n_1 > n_h$. Some numerical examples for platinum inclusions are cited. When $r_o = 10^{-4}$cm, $E_L = 20$ (J/cm^2), and $\tau = 30$ns, then an effective focal length due to the lens effect occurs at $\tau \sim 3\mu$s and is about $f \sim 14$ cm. But the tensile stress at $t = \tau = 30$ns exceeds the theoretical strength of the host before the lens effect becomes most important. Consider now another example for Pt in which the maximum tensile stress is less than the theoretical breaking strength of the glass host. When $r_o = 10^{-4}$cm, $E_L = 0.33$ (J/cm^2). $\tau = 30$ns, and $T_h(r_o,\tau) = 600°C$, the effective focal length attains a value of about 10^4cm for times $t \sim 3\mu$s. This latter focal length is very long.

Hence, the model predicts that the lens effect arising from heated inclusions probably does not cause damage. Those cases for which the maximum tensile stress is less than the theoretical tensile strength of the glass have minimum effective focal lengths which are much greater than the dimensions of Nd-doped glass elements used in present laser systems. In those cases for which the minimum effective focal length is comparable to the size the host, the tensile stress exceeds the theoretical strength of the glass and probably causes damage before the lens effect becomes large enough to heat another inclusion or to initiate an intrinsic damage mechanism such as self-focussing.

In conclusion, the model enables one to answer qualitatively many questions concerning laser damage due to absorbing centers and concerning the detection of such centers before they cause damage.

REFERENCES

1. H. S. Bennett, "Inclusions in Laser Materials," to be published.
2. H. S. Bennett, "Heat Diffusion near Absorbing Centers in Laser Materials," to be published.
3. B. Boley and J. Weiner, Theory of Thermal Stresses (John Wiley and Sons, Inc., New York, 1960)

4.3.3 Degradation of Laser Materials

Crystal Defect Studies on Laser Materials

4.3.3.1. EPR Measurements on Normal and Orange Ruby

R. F. Blunt, T. Chang, and M. I. Cohen
Inorganic Materials Division
Institute for Materials Research

Objective

This investigation is a study of the causes responsible for degration of performance of solid state lasers. The effort has been directed largely to a study of orange degradation of laser ruby, by EPR and optical means. (See NBS Technical Note 531 for previous report).

Technical Approach

In the work described here, the emphasis has been shifted away from optical measurements to some extent, with greater effort expended on the EPR and with the addition of magnetic susceptibility measurements. (The latter is described in a separate section of this report). The activities include:

1. The study of the $\Delta m = 2$ EPR transition in ^{60}Co irradiated ruby has been extended to include a measure of the line intensity as a function of the Cr concentration. The results are compared with the previously reported "orange" coloration dependence.

2. The Cr^{3+} EPR line intensity of the -3/2 → -1/2 transition was measured carefully under controlled conditions on various Cr concentrations. This procedure is a potential analytical tool for Cr^{3+} concentration determination and as such is a means of study of loss of normal Cr^{3+} in "orange" degraded ruby (e.g. conversion to Cr^{2+} and Cr^{4+}).

The following experiment is supported in part by ARPA and logically belongs to this list.

3. Magnetic susceptibility experiments were made on rubies of several concentrations as a means of direct measurement of the Cr^{3+} concentration. Measurements were made with and without microwave (EPR) saturation of the Cr^{3+} ground state levels to take into account the contributions to the paramagnetic susceptibility which arise from species other than Cr^{3+}. Finally, measurements were made after ^{60}Co irradiation to check on the reduction of Cr^{3+} concentration in the damaged samples. (These results are discussed in a separate section of this report).

Experimental Results

In a recent report (see NBS Technical Note 531) we described the orange coloration of X-irradiation damaged ruby as studied by optical absorption. The absorption coefficient of one prominent band, with a maximum at about 0.47 μm, was shown in crystals colored to saturation to depend on the Cr concentration, with maximum damage at about 0.1 mol% Cr in Al_2O_3. The total added coloration at about 0.47 μm decreases at both higher and lower concentrations.

One effort at identifying the centers responsible for this coloration was reported. It involved the study of a $\Delta m = 2$ EPR transition in "orange" ruby. These measurements have been continued.

A. The Study of the $\Delta m = 2$ Transition

One type of paramagnetic center induced by high energy ionizing radiation is one that yields the $\Delta m = 2$ transition observed in N^{3-} compensated ruby by Hoskins and Soffer(1) and in X-irradiated ruby by Mason and Thorp(2). They attributed the EPR absorption to Cr^{4+} in Al_2O_3. The electronic configuration of Cr^{4+} is $3d^2$, hence the electronic spin is one. The axial component of the crystalline field splits the $m_s = \pm 1$ and $m_s = 0$ levels by about 7 cm^{-1}. The $m_s = \pm 1$ level will be split in a magnetic field and the transition between the components (i.e. $\Delta m = 2$) is normally forbidden. However, the axial crystalline field mixes the $m_s = \pm 1$ levels, and the transition can be observed in the experimental configuration with the dc and rf magnetic fields both parallel to the c-axis of the sample. The line shape is observed to be asymmetrical and $g = 1.90$.

A set of samples containing 0.35, 0.18, 0.088, 0.035, and 0.007 mol% Cr were prepared. (0.05 wt % Cr_2O_3 is approximately equal to 0.035 mol% Cr). These samples were oriented by X-ray diffraction and irradiated to saturation by ^{60}Co. The flux 2.6×10^3 J/cm^2($\approx 2.6 \times 10^8$ R/cm^2) used was deemed more than sufficient from previous optical measurements. Samples were irradiated at room temperature, stored at room temperature, and kept in the dark except for brief exposure to dim incandescent lights. In addition, all measurements were completed within a few days after irradiation. These precautions were felt necessary to prevent or at least greatly reduce u.v. and thermal bleaching of the centers formed.

The spectrometer was operated at about 9.5 GHz and at liquid helium temperature. The power input to the sample cavity was kept constant for each measurement. The coaxial cable coupling scheme of the cavity assembly(3) enables the coupling to be adjusted just slightly under critical coupling, and the rectangular cavity was operated in a TE_{102} mode. Each sample was cemented at the center of the bottom of the cavity such that the c-axis was along the direction of the magnetic vector of the microwave field. Rotation of the magnet about the fixed

cavity permitted the alignment of B_{dc} parallel to the c-axis.

A typical first derivative curve is shown in Fig. 1 (a) and the absorption line obtained after integration is shown in Fig. 1 (b). On the high field side of the zero-crossing point (or the peak of the integrated curve), the absorption line is well defined and extends about 3 millitesla. The shape is distinct and almost the same for all samples, but on the low field side, a long tail is observed. For the 0.007% sample, this tail extends more than 8 millitesla. For more concentrated samples, the tail becomes long and flat. In the 0.088% sample, the tail in the derivative curve (i.e. the signal in the detection method employed in our spectrometer) was not measurable beyond about 3 millitesla. The integrated intensity does not fall very much below the peak value in this case, thus it is apparent that the low field tail extends much further than is observable and that the apparent areas of the absorption lines are too small for the higher concentrations.

It is also found that the signal is weaker for the heavier doped samples. The gain of the lock-in amplifier had to be set a factor of 10 higher for the 0.18% sample than for the 0.007% sample in order to obtain a measurable signal. For the 0.35% sample, it was just barely possible to determine the position of the absorption line only. Further difficulty was encountered as numerous other lines appeared with samples of 0.088% doping or greater. They increased rapidly both in number and intensity with concentration. The $\Delta m = 2$ signal was located on the wing of an intense line in the case of the 0.35% sample, for example.

Extraneous lines (aside from the Cr^{3+}) appeared in all samples. In the most favorable conditions for the $\Delta m = 2$ line, these extra lines were not detectable in the two dilute samples. At proper power level and temperature, the other lines could be much stronger than the $\Delta m = 2$ line. The origin of these other lines was not investigated. It is quite possible that some of these are Cr^{3+} pair lines, and that some

may be from other paramagnetic species such as color centers.

The absorption lines obtained by single integration (see Fig. 1 (a) and (b)) were integrated a second time to get the area or total line intensity. The areas were then normalized for amplifier gain and sample volume. These final numbers are presumed to be a relative measure of the $\Delta m = 2$ transition. The results are listed in Table I, and are also plotted as the four points on Fig. 2. The solid curve in Fig. 2 is the added optical density at 0.47 μm as presented in the last report (NBS Technical Note 531), plotted as a function of mol% Cr.

The EPR measurements suggest that the centers responsible for the $\Delta m = 2$ transition follow generally the same type of concentration dependence of the orange coloration. The maximum EPR intensity would appear to occur at lower Cr concentration than that observed in the optical data. From the discussion in the next experiment, the error in the $\Delta m = 2$ measurement of intensity may be 20%. Also from the above discussion of line shape, the true area of the line probably is larger than indicated, in the more heavily doped samples. Moreover, the optical measurements were performed at room temperature rather than at 4 K as were the EPR, which may cause some discrepancy.

The similarity in shape between the plots in Fig. 2 of the $\Delta m = 2$ EPR transition line intensity and the added optical density as a function of the Cr concentration certainly suggest that they may have a mechanism in common. It is not possible to suggest a definite model at this time for this nor is it possible to offer models for the EPR line and the orange coloration. We can only repeat earlier statements that the coloration is too intense to be explained by Cr valence changes, i.e. the required oscillator strength would be unreasonable. Thus the color could most easily be explained as due to unspecified color centers. The EPR line is related but not necessarily due to the same center.

B. Cr^{3+} EPR Measurements

In this experiment, an attempt has been made to verify the validity of the quantitative analytical application of the EPR technique as described in the previous experiment. The Cr^{3+} EPR lines were measured in the same way with appropriate modifications in procedure. The Cr^{3+} EPR spectra has been studied extensively by various investigators at various temperatures. E. O. Schulz-du Boise (4) has given a theoretical calculation and experimental verification of all the EPR levels and transitions, and angular dependencies. R. P. Bashuk, et.al (5) attempted to correlate the results of the determination of Cr concentrations in ruby by several methods. The EPR measurement seemed in good agreement with other measurements.

The samples were cemented on the side wall of the cavity with the c-axis horizontal. This permitted the c-axis to take all possible orientations with respect to B_{dc} and also made $B_{dc} \perp B_{rf}$. All measurements were made at liquid nitrogen temperature.

The first of two sets of samples measured were the $\Delta m = 2$ set described earlier. For each sample, several Cr^{3+} lines were measured, integrated, and normalized for sample volume. The line "intensities" so obtained failed to fit the presumed linear dependence on concentration and the errors seemed to be about 20%. It was subsequently decided that the size and shape of the samples varied too much to ensure equal coupling into all samples. This was indicated by changes in cavity resonant frequency from sample to sample that seemed excessive. In addition, difficulties prevented precise reproducible location of samples in the cavity, and the Cr concentrations were not well known.

The second set of samples were then prepared from the optical samples used for the solid curve in Fig. 2. The concentrations had been measured by optical absorption. All samples were cut to the same size, shape, and crystallographic orientation. In each case the sample was placed in the cavity with some care. The $-3/2 \rightarrow -1/2$ transition with $B_{dc} \perp$ c-axis was chosen as particularly favorable for a number of reasons. The results are given in Table II and the integrated

intensities plotted in Fig. 3. The resonant frequency of the cavity is seen to change little from sample to sample.

The concentration in sample X, (0.007%), is known to be in doubt owing to the inconveniently low optical density of the original optical sample from which it was prepared. For sample A, (0.34%), the determination was also in error, from some unknown cause. The remaining points follow a straight line through the origin as expected, but with the points for higher concentrations falling below the straight line as indicated by the dotted line. It is likely that the upper points do not obey a linear law but too few points are available to determine other than the departure from the lower solid line.

It is known that Cr^{3+} pairs start to become appreciable above about 0.1 mol% Cr(6). Thus, the normal Cr^{3+} line intensities would be reduced from the expected values at higher concentrations. Two other interesting possibilities exist. The microwave power and the modulation field were both maintained the same for all measurements. The power and the per cent of modulation may be too low for the more concentrated samples because it was observed that the lines were broader. Thus, the ions in the outer wings of the line may not have been integrated due to background (noise, nearby lines, and drift). Somewhat opposite reasoning may be applied to the 0.007% sample in which case the power may have been too high causing experimental line broadening and a high area to concentration ratio.

The results presented here would indicate that for concentrations below about 0.14 mol% it is possible, by this method, to obtain relative concentrations to within 2%. It should further be pointed out that the cavity was assembled and disassembled for each sample mounting and that unlike other similar measurements(5) reference samples (e.g. DPPH) permanently attached to the cavity were not necessary. We feel that the reliability, reproducibility, and potential accuracy (with proper calibration) is well demonstrated. Further, the extension of this method to considerably smaller concentrations and even to other

paramagnetic species is quite feasible.

Table I

The comparison of EPR Absorption of the $\Delta m = 2$ Transition in ^{60}Co irradiated ruby with the Cr concentration.

Sample Concentration mol% Cr	Normalized Integrated Area (arbitrary units)
0.35	----
0.175	45
0.088	410
0.035	1500
0.007	690

Table II

The measurement of the integrated area of the EPR absorption line of the $m_s = -3/2$ to $-1/2$ transition of Cr^{3+} in ruby.

Sample	Concentration (mol % Cr)	Microwave Frequency (GHz)	Area of EPR Line (arbitary units)	Area / conc. x 100
X	0.007	9.5384	66	94
L	0.04	9.5384	230	58
E	0.076	9.5380	436	58
B	0.075	9.5386	447	60
W	0.11	9.5337	655	60
Y	0.14	9.5342	820	59
H	0.20	9.5336	960	48
D	0.38	9.5381	1500	40
A	0.34	9.5398	3260	96

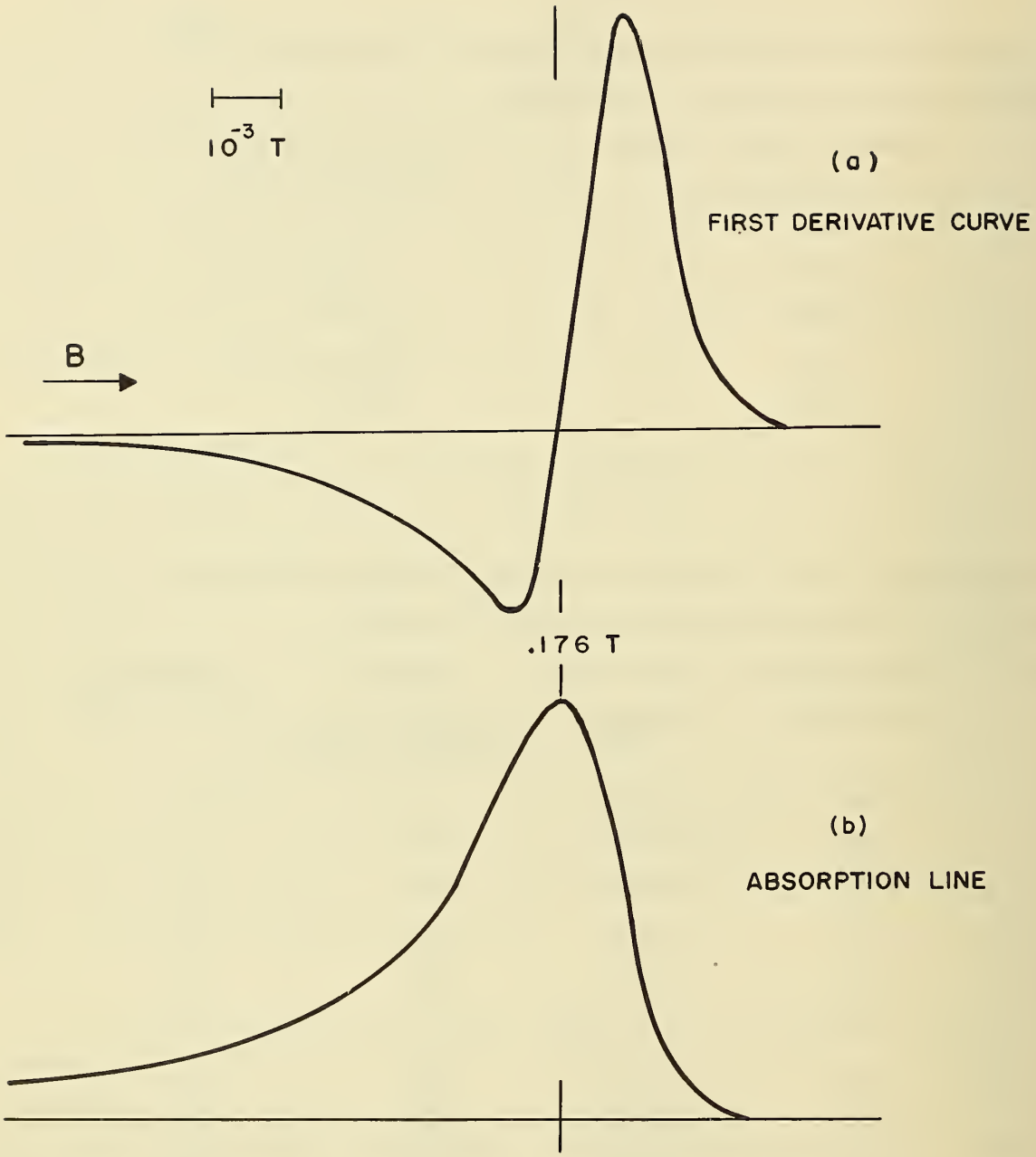

Fig. 1. The $\Delta m = 2$ EPR transition in γ-irradiated ruby, ordinate in arbitrary units vs. magnetic induction (a) experimental derivative curve; (b) absorption line obtained by integration. Induction, T, in Tesla.

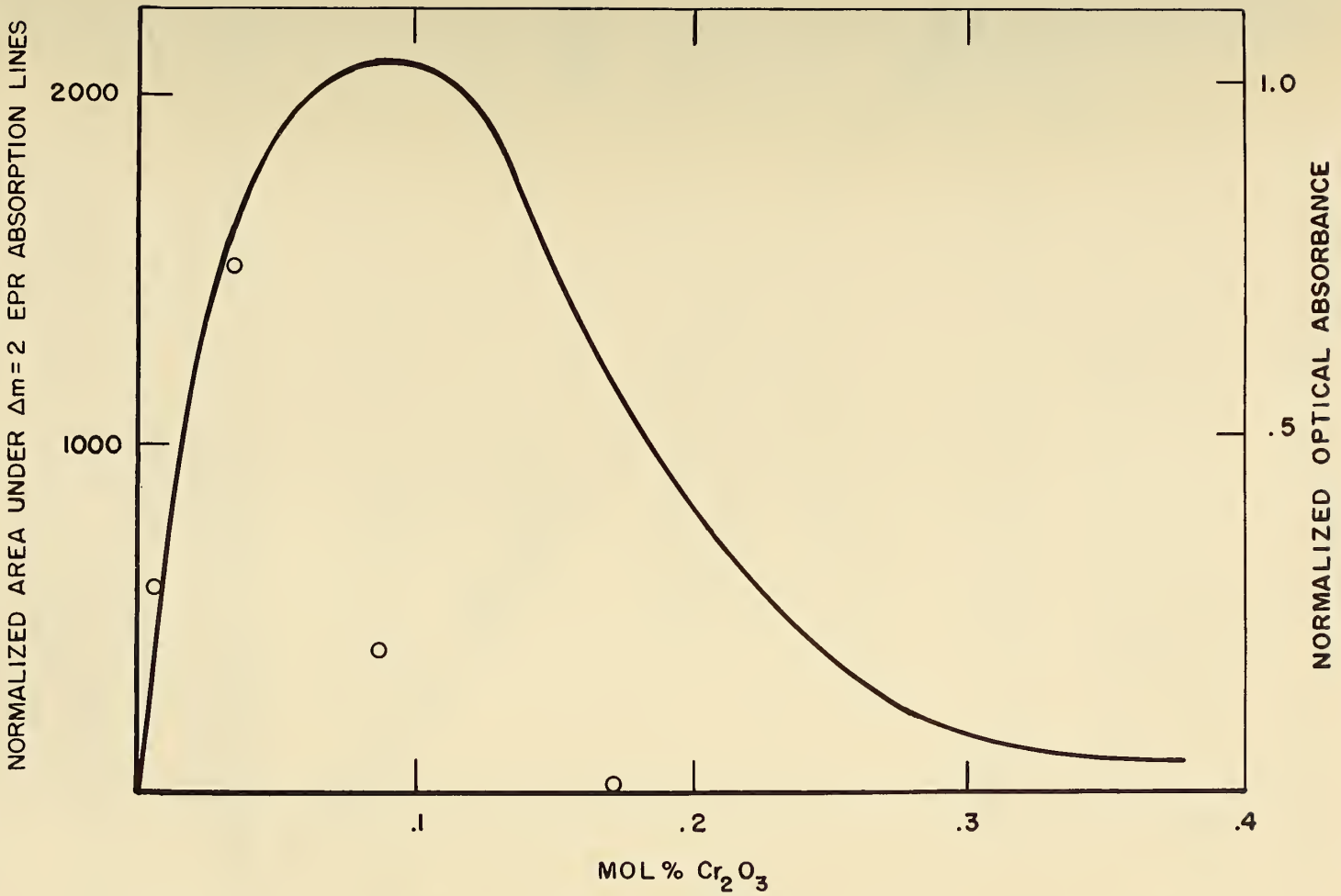

Fig. 2. Comparison of the integrated Δm = 2 EPR absorption with the corresponding added coloration (0.47μm) in γ-irradiated ruby plotted vs. mol% Cr. The circles, o, represent the EPR data.

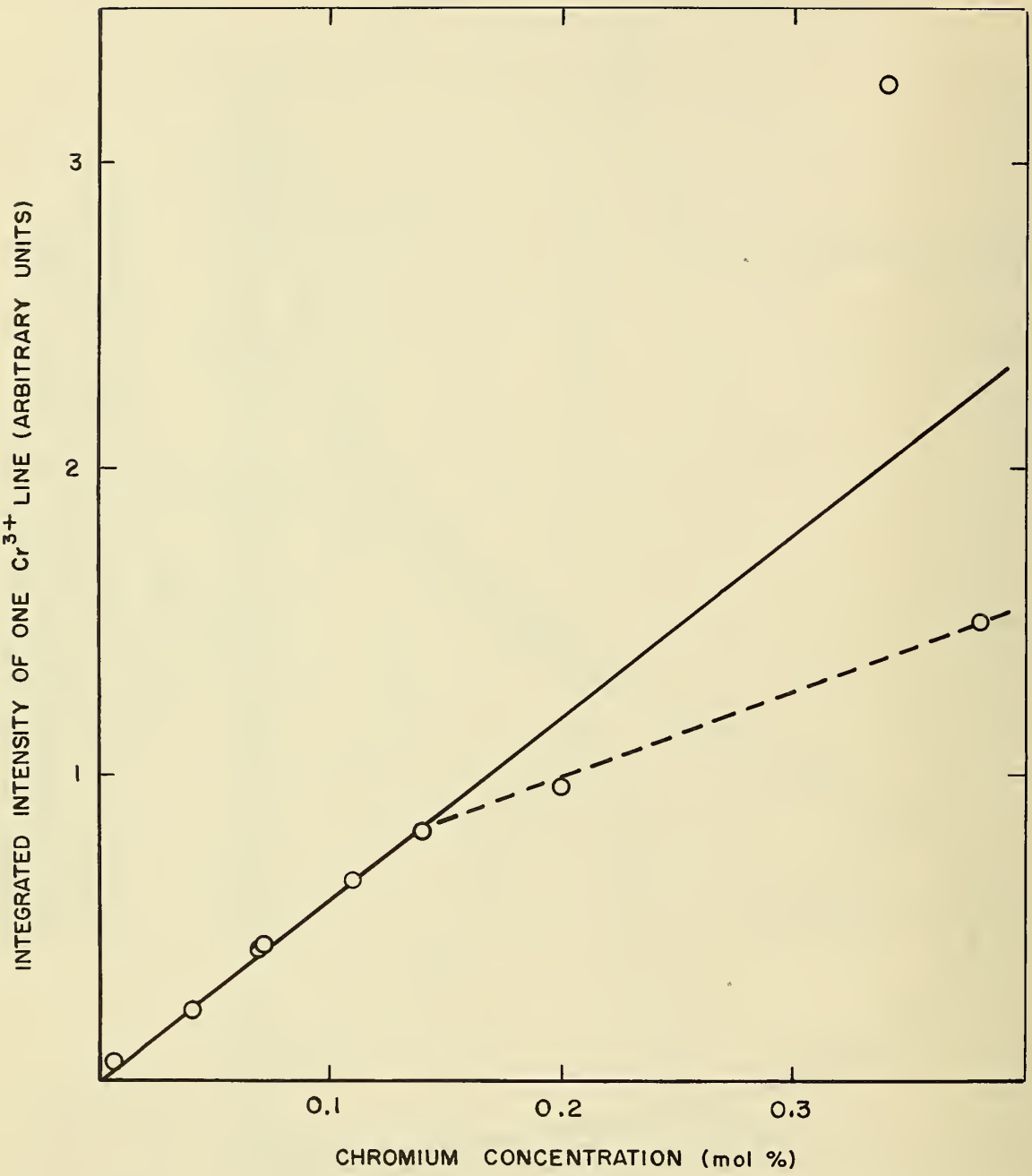

Fig. 3. Integrated intensity of the $-3/2 \rightarrow -1/2$ Cr^{3+} EPR line in ruby vs. mol% Cr. Measurements made at liquid N_2 temperature, X-band frequencies, and with $B \perp c$.

REFERENCES

1. R. H. Hoskins and B. H. Soffer, Phys. Rev. 133, A490 (1964).
2. D. R. Mason and J. S. Thorp, Proc. Phys. Soc. (London) 87, 49 (1966).
3. E. O. Schulz-du Bois, Bell System Tech. Jour. 38, 271 (1959).
4. T. C. Ensign and T. Chang, Rev. Sci. Instr. 40, 268 (1969).
5. R. P. Bashuk, et al., Zhurnal Prikladnoi Spektroskopii 5, 172 (1966).
6. H. Statz, L. Ramai, M. J. Weber, G. A. Demars, Jour. Applied Phys. 32, 2185 (1961) and J. C. Gill, Proc. Phys. Soc. (London) 79, 58 (1962).

4.3.3.2. Optical Absorption Determination of Chromium in Ruby

R. F. Blunt
Inorganic Materials Division
Institute for Materials Research

Objectives

The objectives of this investigation were:

1. The Cr^{3+} concentration determination in several laser quality ruby crystals following the optical method of Dodd, Wood, and Barns (1).

2. The correlation of the above results with analyses made by other methods, both previously reported and current.

3. A new determination of the Cr^{3+} optical absorption coefficents in ruby.

Experimental Results

The method used[1] consists of measuring the absorption coefficient at maximum absorption for the two major bands near 0.40 and 0.56 μm. Measurements must be made for E⊥c, E∥c, or both, and are made at room temperature for convenience. As a further convenience most measurements are made for E⊥c only, since this direction is always available in samples having arbitrary orientation of the c-axis. Beer's Law is presumed to be valid, that is, the absorbance, A, is expressed by: $A = \log_{10} (Io/I) = 0.434\ \mu\ C\ d$, after appropriate corrections to the experimental A are made for sample surface losses. It is customary to give the sample thickness, d, in cm, and the Cr concentration, C, in wt. % Cr_2O_3, thus μ can be described as the absorption coefficient (cm^{-1}) for 100 wt. % Cr_2O_3.

The absorption is presumed to be due entirely to the well-studied Cr^{3+} ions, and it is assumed that the wavelength regions around 0.32 and 0.68 μm have no bulk absorption. In this method, a smooth curve connecting these two regions is used as a surface loss baseline from which the Cr^{3+} band maxima near 0.40 and 0.56 μm can be determined. It can be shown, that for materials with refractive indices less than 2, this method of surface correction is very good, providing, of course, that the smooth curve is a reasonable approximation for the bulk material without the absorption bands.

We find that for ruby with well polished surfaces, a straight line of absorbance vs. wavelength joining, say, 0.32 and 0.68 μm is usually adequate. This straight line is approximately tangent to the presumed baseline at both points. In those cases where the surfaces are not good, and large surface losses result, the slope at 0.32 μm is definitely greater than at 0.68 μm and a more complicated baseline is needed. The one chosen is made by estimating the slope and absorbance values at 0.32 and 0.68 μm and joining the two points with the relation:

$$A_\lambda = A_{.32} - m_{.32} (\lambda - 0.32) + b (\lambda - 0.32)^n,$$

where $m_{.32} \geq 0$ is the slope at .32 μm. The constants $b \geq 0$ and $n \geq 1$ are calculated to yield the "correct" slope and absorbance at 0.68 μm.

Both baseline methods were employed at various times in the course of these measurements and the results of the less simple curve are believed to be more realistic and reliable in those cases where the need for a change of slope is clearly indicated. For even poorly polished samples the variable slope formulas resulted in at most a 3% increase in corrected absorbance, A, over that provided by the linear baseline. In all cases the samples measured were restricted to those having bands of corrected optical density of at least 0.3, preferably more than 0.5, or in one case slightly over 1.0. Very well-polished samples really required only the linear correction. On several occasions, samples were measured that had not been polished at all, merely ground to size. The results appeared unreliable, and subsequent measurements on the samples after polishing yielded values differing by 10 to 15% from the earlier ones. Thus the desirability of polished surfaces is quite evident, yet cases where a rough check of chromium concentration is needed would indicate the convenience of the linear baseline method on unpolished samples.

Measurements of chromium concentration, presumably as Cr^{3+}, on a number of samples are given in Table I. The absorption coefficients used are the ones in the reference(1) $\mu_{.4,\perp} = \mu_{.56,\perp} = 47.1\ cm^{-1}$; the other values $\mu_{.4,\parallel} = 89.0\ cm^{-1}$, and $\mu_{.56,\parallel} = 15.8\ cm^{-1}$. The quoted values for the R lines were not used or considered in these measurements. $\perp$ and $\parallel$ designate E perpendicular or parallel to the c-axis respectively. We measured both bands and took the average. (The two values agreed within 2% at worst). Since many of these samples came from boules previously reported on, we repeat the earlier results for comparison and use the same sample identification. We also include measurements obtained by a magnetic susceptibility method discussed elsewhere in this report, and three new activation analyses.

Concentrations are given as wt% Cr_2O_3. The C_n refer to the neutron activation analyses (NA), the C_o and C_x to the current optical and susceptibility measurements respectively. The C_n* values are very recent determinations.

The samples designated "05" were cut from the nominal 0.05% boule (Section 4.4.1.1. of NBS Tech. Note 531) a boule about 1" in diameter. The position of the NA sample relative to the optical sample is unknown. The 050, and 100 boules were nominally 0.05, 0.075, and 0.100% rods about 1/2" in diameter. These were discussed in Section 3.6.5. of NBS Tech. Note 514. All four boules were 60° crystals. The 0.5V samples were adjacent pieces from a red Verneuil ruby of unknown origin.

Corresponding samples cut from the three boules are identified by parentheses. Slices number(1) through(7) are adjacent pieces near one end of the boule, and(3) was cut to have large parallel(001) faces. Slice(8) was cut perpendicular to the boule axis several inches below the above mentioned pieces. Slice(9) was near the opposite end from(1).

The optical values, in most cases, seem to be considerably smaller than the activation determinations and consistently larger than those the susceptibility method gives. The reasons for these discrepancies are not understood. The optical method is designed to measure only Cr^{3+} ion. Other valence states, or other transition metal ion impurities, would either not be detected or would introduce errors unless they resulted in well-defined extraneous bands. We assume that for laser quality ruby, Cr^{3+} ions are the principle source of the optical absorption bands and that the only likely error would arise because of the presence of Cr in other valence states, which would not be separately identified if present in small amounts. (A loss or gain of Cr^{3+} in a given sample would be measurable under favorable circumstances.) Within these limitations, optical absorption offers a very convenient method for the analysis of Cr in ruby.

The precision available from optical absorption is 2 to 3% and the method permits, when small apertures are used, the study of sample inhomogeneity. Some idea of the inhomogeneity has been indicated in Table I, although little effort at detailed "mapping" has been

attempted. The series (3) slice permitted measuring three places and a variation of several per cent was observed; the series (8) disks were measured in the center and four places around the edges. In the latter, the edge values were 5 or 6% higher than the center values. Average values were used in Table I. The accuracy of the method is determined largely by the reliability of the absorption coefficients that must be determined by other analyses.

TABLE I

Chromium Analysis (Wt% Cr_2O_3) of Ruby Crystals by Activation Analysis, C_n; Optical Absorption, C_o; and Magnetic Susceptibility Measurements, C_χ.

METHODS

Crystal and Sample	C_n	C_o	C_χ	C_o/C_χ
05-NA	0.0443			
05 "¼" cube		0.055		
05 "x"	0.0462*	0.054	0.044	1.21
050 - (4)	0.059			
050 - (3)		0.048		
050 - (8)		0.053		
	0.072			
050 - (9)	0.065			
075 - (4)	0.078			
075 - (3)		0.067		
075 - (8)		0.072		
075 - (9)	0.086			
100 - (4)	0.104			
100 - (3)		0.083		
100 - (1)	0.0832*	0.088	0.073	1.21
100 - (5)		0.085		
100 - (8)		0.087		
100 - (9)	0.098			
0.5V		0.44	0.37	1.20
0.5V - NA	0.441*			

The quoted μ values (1) were assigned standard deviations of about 10%. One other determination can be cited (2) for the 0.56 μm band, in which a value equivalent to 55 cm^{-1} was reported (to be contrasted with the 47.1 cm^{-1} used in Table I). This uncertainty together with the

convenience and higher "precision" of the optical method, would make a more accurate re-determination of absorption coefficients desirable. Previous analyses(1,2) in principle give total Cr as do the activation analyses reported here, as opposed to the optical method which probably responds only to the Cr^{3+} ions in the calibrating samples. The magnetic susceptibility method is believed to be particularly favorable for determining the normal unpaired Cr^{3+} ions in laser quality ruby. This method is described in another section of this report on "The Analysis of Cr^{3+} in Orange Ruby by Magnetic Susceptibility Measurement." It offers apparent precision on these samples of about 2% and in principle is an absolute method; that is, the measured susceptibility is expressed as a known formula containing well determined physical constants, temperature, and the number of Cr^{3+} spins. Further, in the three samples measured, the ratio of the optical value to the susceptibility value (both made on the same sample) was constant within 2%, with an average of 1.21.

The lower concentrations for the susceptibility measurements as compared with the other chemical analyses (directly or indirectly) raises several interesting questions which might warrent further investigation. Such questions are exemplified by the possibility of an appreciable fraction of the Cr not being in the Cr^{3+} state or that an appreciable fraction of the ions are strongly coupled into anti-ferromagnetic pairs. Also the possibility of fortuitous sample inhomogeneity confusing much of the data cannot be ruled out.

The excellent tracking of the ratio C_o/C_χ adds considerable confidence in the susceptibility method. If one then assumes that the concentrations so determined (column 3 of Table I) are correct, new values of the calibration coefficients can be calculated. The quoted equality of the $E_\perp c$ constants for the 0.40 and 0.56 μm bands seems reasonable. Other relative checks were made on the "$\frac{1}{4}$" cube, which had parallel faces containing the c-axis thus permitting E//c measurements. From these and the measurements of Table I we calculate: 56.8, 56.8, 104.7, and 18.2 cm^{-1} respectively for $\mu_{.4,\perp}$, $\mu_{.56,\perp}$, $\mu_{.4,\|}$, and $\mu_{.56,\|}$.

REFERENCES

1. D. M. Dodd, D. L. Wood, and R. L. Barns, J. Appl. Phys. 35, 1183 (1964).
2. R. P. Bashuk, et al., Zhurnal Prikladnoi Spektroskpoii 5, 172 (1966).

4.3.3.3. Analysis of Cr^{3+} in Orange Ruby by Magnetic Susceptibility Measurements

R. F. Blunt, G. A. Candela, R. A. Forman, and A. H. Kahn
Inorganic Materials Division
Institute for Materials Research

Objective

The objective of this work was the investigation of the magnetic susceptibility of paramagnetic spins in ruby as a method of Cr^{3+} determination. The following experiments were planned:

1. Precision bulk magnetic susceptibility measurements on each of several crystals containing different concentrations of Cr.
2. Simultaneous and selective microwave saturation of the ground state levels of Cr^{3+} to give a positive identification of the contribution to the susceptibility of the Cr^{3+} ions.
3. The measurements to be repeated on the same samples after ^{60}Co irradiation as a possible means of determining loss of Cr^{3+} associated with the resulting coloration.

This work has been supported in part by the Advanced Research Projects Agency.

Experimental Results

Pure sapphire is diamagnetic and hence paramagnetic centers such as substitutional Cr^{3+} can be expected to give predictable and measurable susceptibility even when present in concentrations such as

0.05 wt % Cr_2O_3. Additional paramagnetic centers can, of course, make appreciable contributions and have to be allowed for if susceptibility is to be used as an analytical tool.

Theoretical derivations(1,2) give expressions applicable to our case using the assumption of isolated substitutional Cr^{3+} ions in the trigonal α - Al_2O_3 lattice. In our experimental conditions, the susceptibility, χ, is given to a good approximation by: $\chi = \frac{NC}{T + \Delta}$, where C is a quantity involving only fundamental constants and the g value for the ions and N is the number of ions in the sample. The g values for Cr^{3+} in ruby are very precisely known. Δ can be considered, in this simple discussion, as a constant that can be determined by making measurements at several temperatures, and it is anisotropic. The Cr^{3+} concentration is calculated from the sample weight and the value of N obtained from the above.

The apparatus used has been described previously(3). It employs the Faraday method but in addition has the sample suspended in the Ka-band microwave cavity thus permitting simultaneous microwave resonance. The conditions for resonance in these measurements were $B \perp$ c-axis with B = approximately 0.05 tesla, such that one Cr^{3+} resonance occurs at a microwave frequency of 14.1 GHz. Under these conditions it is possible to resonate one transition and get some "pumping" to all levels via cross relaxation. Thus when the spin-lattice relaxation time is long enough, all four ground state levels can be saturated, thereby removing these ions from the spin system available for susceptibility.

Three samples about 300 mg each were measured, having nominal concentrations of 0.05, 0.10, and 0.50 wt % Cr. Bulk susceptibility was measured at 300K, 78K, and several temperatures between 4.2 and 2K. The concentration of paramagnetic ions was sufficiently low so that the (diamagnetic) susceptibility measured at 300K could be used for the lattic diamagnetic correction. The corrected χ values for low temperatures thus contained normal Cr^{3+} contributions from which the

concentration could be calculated plus additions from extraneous paramagnetic centers. The diamagnetic susceptibilities agreed well with published values for sapphire. Finally, a sample of extremely pure sapphire grown at NBS by H. S. Parker was measured down to 2 K. A susceptibility value of -0.32×10^{-6} cm^3 gm^{-1} was obtained. The expected, essentially temperature independent diamagnetism also confirmed the corrections made on the ruby.

Microwave saturation experiments were performed on each of the three ruby samples at 4.2 K and below. The degree of saturation was taken as the fraction of the total bulk paramagnetic susceptibility that was removed at the maximum microwave power used. Both high temperature and high concentration would tend to decrease spin-lattice relaxation time and limit the degree of saturation. Extraneous paramagnetic ions, i.e. ions other that Cr^{3+} in normal substitutional sites, would not be expected to resonate and hence could not be removed from the spin system. These ions would, therefore, reduce the degree of saturation. The 0.5% sample showed considerable saturation, even at 4.2K. At near 2 K, the following values were obtained for the degree of saturation: 99.6%, 97.4%, and 94% for the 0.05, 0.1, and 0.5 samples, respectively. In the case of the 0.05% sample the saturation was essentially 100% at only about 1/3 of the maximum power with no further change with power increase. The saturation of the 0.1% sample may not have reached its maximum value at the maximum microwave power, while this was quite clearly the case for the 0.5% sample. We attribute the lack of approximately 100% saturation in all three samples to fast relaxation in the more concentrated samples or to the danger of overheating the sample, rather than to the presence of extraneous ions. We conclude, therefore, that the measured bulk susceptibility is due almost entirely to largely isolated substitutional Cr^{3+} ions, and that the measured χ can be used to calculate the concentration.

The 0.05 and 0.10% samples were colored orange by a "saturation" irradiation by ^{60}Co and measured. No detectable change in bulk susceptibility was observed. Attempts at microwave saturation yielded very

small reductions in χ, which we attribute to very fast relaxation processes produced by the irradiation damage, hence giving no useful information. The susceptibility data for the orange ruby were plotted on the corresponding graph obtained for the samples before irradiation and the agreement was clearly within 1% at worst. One possible model for the damage would be one in which Cr^{3+} was converted to Cr^{2+} and/or Cr^{4+}. Both of these are expected to have susceptibilities distinctly different from Cr^{3+}, the first higher and the second lower. It would ve very attractive to conclude from the small change, that the loss in Cr^{3+} would be less than 1%. However, when one considers various possible defects that could be generated by the γ-irradiation, the magnetic properties of which are unknown, it is obvious that no real conclusion about valence change can be made. A large reduction in χ would certainly have been suggestive of Cr^{3+} loss. The only conclusion that can be drawn is that the lack of change does put a considerable constraint on the magnetic properties of any model proposed. It does seem most unlikely that any appreciable changes in, additions to, or deletions from the paramagnetic centers originally present would result in a net negligible overall susceptibility change. Such coincidences are unlikely but could happen.

Figure 1 is a plot of χ^{-1} vs. T. The extrapolation of χ^{-1} to zero gives a value of Δ at the intercept with the abcissa. The slope of each curve is in fact the product NC from which the concentration can be calculated. Plotted along with the $B_\perp$ c-axis data are two sets of data taken for $B\|$ c-axis. It is seen that $\Delta_\perp = -4K$ and $\Delta_\| = 0$ K. Theory(1) predicts that these values should be -.1 and+.2K, respectively, and data in the literature(4) is reported to be in accord with these. An additional measurement was made as a check on this apparent discrepancy. It was done on an adjacent piece of the same 0.1% boule at essentially zero field by the mutual inductance method. The measurement was kindly performed by B. W. Mangum of the NBS Low Temperature Section. This method does not afford an absolute calibration hence the data was plotted to a convenient arbitrary scale, but the intercept is in agreement with that obtained at a much higher field.

The apparent discrepancy between the theory for isolated ions and the observed behavior at low temperature is not understood at this time. It should be pointed out that the difference, from the standpoint of Fig. 1, is equivalent to the addition of an isotropic antiferromagnetic susceptibility of such magnitude as to shift the curves over about 0.2 K. The total anisotropy, that is $\Delta_{\parallel} - \Delta_{\perp}$, is observed as 0.4 K rather than the predicted 0.3 K. However, there is no reason, that we can see, how the above difficulty could have appreciable effect on the validity of the determination of the number of Cr^{3+} spins in these samples.

The sensitivity and reproducibility of the susceptibility measurements at 4.2 K and below were sufficiently good to give a resultant Cr^{3+} determination that appears to be good to 1%. The values obtained were: 0.044, 0.073, and 0.37 wt % Cr_2O_3, respectively for the 0.05, 0.10, and 0.5% samples. These were consistently lower than the values (respectively 0.054, 0.088, and 0.44%) obtained on these identical samples by the optical absorption method discussed in another section of this report. This latter method, although capable of excellent reproducibility, is only relative and requires a calibrating constant which might very well be in error. It is interesting to note that the ratios of the optical to susceptibility values were constant within 2% for the three samples.

These analyses, as well as neutron activation analyses are summarized in Table I of the section of this report on "The Optical Absorption Determination of Cr in Ruby."

We believe that this susceptibility method offers a precise and direct method of determining the Cr^{3+} concentration in ruby. It very likely has potential use in other systems in which a dilute ion of appropriate configuration is in a diamagnetic lattice.

REFERENCES

1. M. H. L. Price, Nuovo cimento Suppl. 6, 817 (1957).
2. H. L. Davis, Z. Physik. Chem. 16, 213 (1958).
3. G. A. Candela and R. E. Mundy, Rev. Sci. Instr. 36, 338 (1965).
4. K. Brugger and J. G. Daunt, Z. Physik. Chem. 16, 203 (1958).

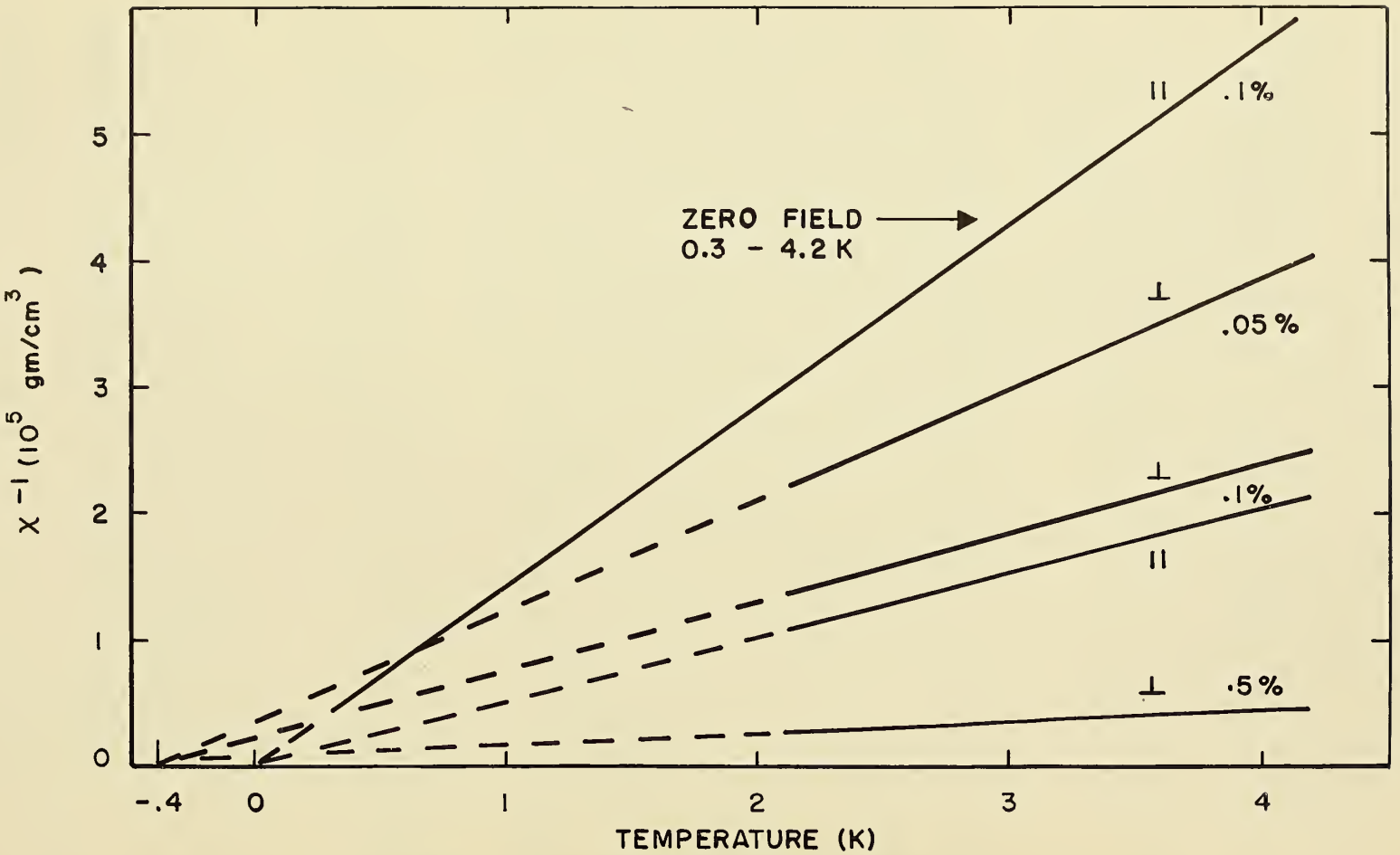

Fig. 1. Magnetic susceptibility, χ, plotted as χ^{-1} vs. temperature for several ruby crystals. Nominal wt. % Cr_2O_3 and c-axis orientation to magnetic field is indicated. The "zero field" curve was measured at very low field and plotted with arbitrary ordinate scale for clarity.

Latest developments in the subject area of this publication, as well as in other areas where the National Bureau of Standards is active, are reported in the NBS Technical News Bulletin. See following page.

HOW TO KEEP ABREAST OF NBS ACTIVITIES

Your purchase of this publication indicates an interest in the research, development, technology, or service activities of the National Bureau of Standards.

The best source of current awareness in your specific area, as well as in other NBS programs of possible interest, is the TECHNICAL NEWS BULLETIN, a monthly magazine designed for engineers, chemists, physicists, research and product development managers, librarians, and company executives.

If you do not now receive the TECHNICAL NEWS BULLETIN and would like to subscribe, and/or to review some recent issues, please fill out and return the form below.

(cut here)

Mail to: Office of Technical Information and Publications
National Bureau of Standards
Washington, D. C. 20234

Name _____

Affiliation _____

Address _____

City _____ State _____ Zip _____

☐ Please send complimentary past issues of the Technical News Bulletin.

☐ Please enter my 1–yr subscription. Enclosed is my check or money order for $3.00 (additional $1.00 for foreign mailing).
Check is made payable to: SUPERINTENDENT OF DOCUMENTS.

TN 565

☆ U. S. GOVERNMENT PRINTING OFFICE : 1971 431-994/179

NBS TECHNICAL PUBLICATIONS

PERIODICALS

JOURNAL OF RESEARCH reports National Bureau of Standards research and development in physics, mathematics, chemistry, and engineering. Comprehensive scientific papers give complete details of the work, including laboratory data, experimental procedures, and theoretical and mathematical analyses. Illustrated with photographs, drawings, and charts.

Published in three sections, available separately:

• Physics and Chemistry

Papers of interest primarily to scientists working in these fields. This section covers a broad range of physical and chemical research, with major emphasis on standards of physical measurement, fundamental constants, and properties of matter. Issued six times a year. Annual subscription: Domestic, $9.50; foreign, $11.75*.

• Mathematical Sciences

Studies and compilations designed mainly for the mathematician and theoretical physicist. Topics in mathematical statistics, theory of experiment design, numerical analysis, theoretical physics and chemistry, logical design and programming of computers and computer systems. Short numerical tables. Issued quarterly. Annual subscription: Domestic, $5.00; foreign, $6.25*.

• Engineering and Instrumentation

Reporting results of interest chiefly to the engineer and the applied scientist. This section includes many of the new developments in instrumentation resulting from the Bureau's work in physical measurement, data processing, and development of test methods. It will also cover some of the work in acoustics, applied mechanics, building research, and cryogenic engineering. Issued quarterly. Annual subscription: Domestic, $5.00; foreign, $6.25*.

TECHNICAL NEWS BULLETIN

The best single source of information concerning the Bureau's research, developmental, cooperative and publication activities, this monthly publication is designed for the industry-oriented individual whose daily work involves intimate contact with science and technology—*for engineers, chemists, physicists, research managers, product-development managers, and company executives.* Annual subscription: Domestic, $3.00; foreign, $4.00*.

*** Difference in price is due to extra cost of foreign mailing.**

NONPERIODICALS

Applied Mathematics Series. Mathematical tables, manuals, and studies.

Building Science Series. Research results, test methods, and performance criteria of building materials, components, systems, and structures.

Handbooks. Recommended codes of engineering and industrial practice (including safety codes) developed in cooperation with interested industries, professional organizations, and regulatory bodies.

Special Publications. Proceedings of NBS conferences, bibliographies, annual reports, wall charts, pamphlets, etc.

Monographs. Major contributions to the technical literature on various subjects related to the Bureau's scientific and technical activities.

National Standard Reference Data Series. NSRDS provides quantitative data on the physical and chemical properties of materials, compiled from the world's literature and critically evaluated.

Product Standards. Provide requirements for sizes, types, quality and methods for testing various industrial products. These standards are developed cooperatively with interested Government and industry groups and provide the basis for common understanding of product characteristics for both buyers and sellers. Their use is voluntary.

Technical Notes. This series consists of communications and reports (covering both other agency and NBS-sponsored work) of limited or transitory interest.

Federal Information Processing Standards Publications. This series is the official publication within the Federal Government for information on standards adopted and promulgated under the Public Law 89–306, and Bureau of the Budget Circular A–86 entitled, Standardization of Data Elements and Codes in Data Systems.

Order NBS publications from: Superintendent of Documents
Government Printing Office
Washington, D.C. 20402